**exotech** inc.

3rd Floor, 1901 S. Bascom Ave., Campbell,
California U.S.A. 95008

# AD-A166 757

FINAL REPORT

## DEVELOPMENT AND EVALUATION OF A NUMERICAL SOLUTION OF THE EULER EQUATIONS USING THE GODUNOV METHOD.

TR 8401

NOVEMBER 1984

DTIC
SELECTED
APR 2 3 1986
S D
D

PREPARED BY

S. EIDELMAN

SUBMITTED TO

NAVAL POSTGRADUATE SCHOOL,
MONTEREY, CALIFORNIA, 93943

UNDER CONTRACT

N00014-84-C-0677

86  4   23  000

| REPORT DOCUMENTATION PAGE | READ INSTRUCTIONS BEFORE COMPLETING FORM |
|---|---|
| 1. REPORT NUMBER | 2. GOVT ACCESSION NO. AD-A166 757 | 3. RECIPIENT'S CATALOG NUMBER |

| 4. TITLE (and Subtitle) | 5. TYPE OF REPORT & PERIOD COVERED |
|---|---|
| Development and Evaluation of a Numerical Solution of the Euler Equations Using the Godunov Method | Final |
| | 6. PERFORMING ORG. REPORT NUMBER TR 8401 |

| 7. AUTHOR(s) | 8. CONTRACT OR GRANT NUMBER(s) |
|---|---|
| Shmuel Eidelman | N00014-84-C-0677 |

| 9. PERFORMING ORGANIZATION NAME AND ADDRESS | 10. PROGRAM ELEMENT, PROJECT, TASK AREA & WORK UNIT NUMBERS |
|---|---|
| Exotech Inc. 1901 S. Bascom Ave., Ste. 337 Campbell, California 95008 | |

| 11. CONTROLLING OFFICE NAME AND ADDRESS | 12. REPORT DATE |
|---|---|
| Department of Aeronautics Naval Postgraduate School Monterey, California 93943-5100 | November 1984 |
| | 13. NUMBER OF PAGES 73 |

| 14. MONITORING AGENCY NAME & ADDRESS(if different from Controlling Office) | 15. SECURITY CLASS. (of this report) |
|---|---|
| Office of Naval Research 800 N. Quincy St. Arlington, Virginia 22217 | |
| | 15a. DECLASSIFICATION DOWNGRADING SCHEDULE |

16. DISTRIBUTION STATEMENT (of this Report)

Approved for public release; distribution unlimited

17. DISTRIBUTION STATEMENT (of the abstract entered in Block 20, if different from Report)

18. SUPPLEMENTARY NOTES

19. KEY WORDS (Continue on reverse side if necessary and identify by block number)

Computer Code
Turbomachinery
Time Unsteady Flow

20. ABSTRACT (Continue on reverse side if necessary and identify by block number)

A computer program developed to solve the Euler Equations was applied to a variety of test cases, including turbomachinery cascades and analytical solutions for subsonic and transonic flow. With attention to boundary conditions and grid configuration, it was found the code had a robust capability to analyze unsteady, time dependent flow fields and shock patterns.

DD FORM 1473 EDITION OF 1 NOV 65 IS OBSOLETE
1 JAN 73
S/N 0102-LF-014-6601

# exotech inc.

3rd Floor, 1901 S. Bascom Ave., Campbell,
California, U.S.A. 95008

FINAL REPORT

# DEVELOPMENT AND EVALUATION OF A NUMERICAL SOLUTION OF THE EULER EQUATIONS USING THE GODUNOV METHOD.

## TR 8401

NOVEMBER 1984

PREPARED BY

## S. EIDELMAN

SUBMITTED TO

## NAVAL POSTGRADUATE SCHOOL, MONTEREY, CALIFORNIA, 93943

UNDER CONTRACT

## N00014-84-C-0677

| Accesion For | | |
|---|---|---|
| NTIS CRA&I | | ☑ |
| DTIC TAB | | ☐ |
| Unannounced | | ☐ |
| Justification | | |
| By | | |
| Dist.ibution / | | |
| Availability Codes | | |
| Dist | Avail and / or Special | |
| A-1 | | |

TABLE OF CONTENTS

## 1. INTRODUCTION

In 1981-1983 a computer program was developed which solves numerically two-dimensional Euler equations using the Godonov method (Ref. 1). The program was intended primarily for turbomachinery application, but with modification to the boundary conditions, application to any problem which is modeled by the Euler equations is possible.

This report covers one year of extensive testing of the code for different flow regimes. This testing was done with three main objectives:

a) To gain experience in simulation of the various problems related to the research activity in the Turbopropulsion Laboratory, Naval Postgraduate School, Monterey, California.

b) To test code accuracy by comparing numerical with analytical solutions.

c) To find the source of errors for various numerical simulations and the basic Godunov method in order to reduce these errors.

Some of the results of these experiments with the code were reported in other papers and appear as appendices to this report. Other cases were simulated, but not published, and will be reported here. Some unsuccessful attempts to improve the code accuracy are also described.

The topics studied and the progress made are described in the following sections.

1) The problem of the gradual opening of wave rotor passage.

2) Numerical modeling of the nonsteady thrust produced by intermittent pressure rise in a diverging channel.

3) Numerical techniques for wave rotor cycle analysis (A. Mathur).

4) Development of a grid generation program in order to generate a grid over wedge-arc configuration.

   Test case of the supersonic flow in a channel with arc, wedge, wedge-arc, sinsoidal arc-bumps.

6) Modification of the Godunov method to include shock fitting using the oblique shock wave theory.

7) Development of the one-dimensional code based on Verhoff's method.

8) Modification of the program for cylindrical geometry problems, and modeling of the flow in CDTD.

9) Modeling of the flow in a detonation engine.

10) Development of the SELCO Method.

11) Grid generation for CDTD inlet

# 2. PROBLEMS CONSIDERED

## 2.1 The Gradual Opening in Wave Rotor Passage.

Influence on the flow pattern of the gradual passage opening in the wave rotor was studied on the basis of a numerical simulation. It was found that, in most cases, a significant volume of the passage will have rotational flow, which should lead to the mixing between the driver and driven gases. In some cases, losses will occur as a result of the multiple reflections of the shock and pressure waves from the passage walls. It was shown that the interface between driven and driver gas will be oblique to the passage walls when the passage opens gradually, and that the interface can retain its obliqueness to the walls. The results for the rectangular and skewed passages are reported in Appendix A.

In the case of the skewed passage, the perfect compression of the driven gas with very small mixing losses could be achieved if the channel opens according to a certain formula of the optimum opening velocity. It was found that the velocity of opening could be predicted by the equation:

$$V_{open} = \frac{V_{sh}}{\sin L_{sk}} \tag{1}$$

where: $V_{open}$ = the velocity of the gradual opening
$V_{sh}$ = the shock wave velocity in the driven gas
$L_{sk}$ = the angle of the skewed passage

## 2.2 Numerical Modeling of the Nonsteady Thrust Produced by Intermittent Pressure Rise in a Diverging Channel.

The dynamics of the expansion of detonation products in a diverging channel were investigated numerically. The influence of particular features in the expansion process, such as the presence of reversed flow and propagation of hammer shocks on the production of thrust were examined. Sequential expansions of detonation products were also modeled and it was concluded that in order to maintain a high frequency periodic mode of operation for propulsion applications, the channel should be refilled with ambient air after each expansion. The influence of the ratio of ambient air to detonation products volume on the dynamics of the thrust production and on the impulse generated during the expansion are also reported. The presentation of the results of this investigation is given in Appendix B.

## 2.3 Numerical Techniques for Wave Rotor Cycle Analysis.

With the author's participation, A. Mathur developed a one-dimensional code based on Godonov's method for wave rotor cycle analysis. Because the resolution of the code on the interfaces was poor, it was decided to develop a one-dimensional code based on the random choice method. Non-standard boundary

2

conditions for this problem were developed.  A paper was written and accepted for publication in the proceedings of the ASME Symposium on Nonsteady Flows. The paper is attached as Appendix C.

## 2.4  Development of the Grid Generation Program for Wedge-Arc Configurations.

The grid generation routine, which was used for the cascade and wave rotor simulations did not allow a full control of the grid parameters.  This control was especially needed for the simulation of the test problems, since we wanted to insure that the grids have the same general parameters for the different wedge-arc configurations considered.

A program which allows the grid generation with full control over grid parameters was developed.  The program, with an example of the grid, is given in Appendix D was delivered to the Naval Postgraduate School and stored in an archive file.

## 2.5  Test Case of the Supersonic Flow in a Channel with Arc, Wedge, Wedge-Arc, Sinusoidal Arc-Bumps.

Performance of the Godunov code was tested for numerous supersonic and subsonic internal flow problems.  The tasks included:

a) An attempt to determine what causes the nonsymetrical behavior for subsonic flow case and whether it is possible to increase the accuracy of the basic Godunov code by changing boundary conditions.

b) A comparison of the numerical solution with analytical predictions for supersonic flow.

For subsonic flows it was determined that the main source of errors was slop discontinuity at the corners of the "bump". When the circular arc bump was replaced by a sinusoidal arc "bump", the symmetry of the subsonic solution improved substantially.  This resulted from the fact that in the case of the sinusoidal arc only the second derivatives are discontinuous at the surface. It was found that the boundary conditions at the surface, which are used by the basic Godunov method (solution of the Riemann problem between the physical point and it mirror image with the same pressure and density but with the negative velocity), produce the most consistent results for various problems.  Results for this simulation are shown in Figure 1.  The grid is shown in Figure 2.

Efforts to improve the subsonic flow solution were discontinued when it was realized that a more objective criteria than symmetry of solution was needed.  For this reason, work on supersonic flows was begun, since, for these conditions, some analytical solutions are available.  First, the method for supersonic flow (M = 2.2) in a channel with a 10% thick circular arc "bump was tried. The grid for this case is shown in Figure 3.  In Figure 4 we show results for this geometry when the inlet Mach number is 2.0.  Results are shown in the form of the distributions of the pressure coefficient over the surface of the lower wall of the channel.  Numerical results correspond very well to the analytical in this case.  It was found, however, that when other flow parameters are compared with the analytical solution, there was substantial disagreement between the reslts.  Figure 5 shows the comparison of the pressure coefficient, entropy, density, velocity and Mach number that were

3

calculated numerically with the analytical solution. The comparison is done for supersonic flow with M=1.6 over 5% thick wedge-arc "bump". As shown in Figure 5, the errors are produced mostly on the shock waves and that the largest is the relative error in entropy. The fact that only pressure is simulated accurately was confirmed for the numerous test cases in which the arc thickness and the wedge angle varied in the wide range of values.

## 2.6 Modification of the Godunov Method based on the Shock Fitting using the Oblique Shock Wave Theory.

A shock fitting was attempted to reduce the errors on the oblique shocks. The procedure for fitting was as follows:

1) Calculate the values using Godunov's method.

2) Using oblique shock wave theory, calculate the exact value of the parameters. This calculation is based on the assumption that the pressure is computed correctly by the Godunov method.

3) Substituting values behind the shock for the exact values. It was found that the procedure did not work if it was applied as described above. Many modifications of this prodedure were tried. Some involved interpolation of the values ahead and behind the shock. The last approach did improve the accuracy of the entropy calculation but introduced oscillations.

## 2.7 Development of the One-Dimensional Code based on the Verhoff Method.

A new formulation of the Euler equations and numerical method to solve them were proposed by Verhoff (Ref. 2). A basic code implementing his method for one-dimensional flow was developed. In Figure 6, results are shown for the case of two colliding shock waves in a tube. These results are a reconstruction of the results presented in Ref. 1 in Figure 5. Comparison of these two figures shows that our code implements the basic Verhoff method correctly. The listing of the program is presented in Appendix E.

We were unable to implement the shock fitting in our code. Comparison between the analytical solution and numerical was 10-15% in error for velocity, pressure and density in the region of the shock wave, if the shock was not fitted.

## 2.8 Modification of the Program for Cylindrical Geometry Problems, and Modeling of the Flows in CDTD.

The Godunov code was modified for simulation of the flow with cylindrical velocity. The modified program was used for modeling of the flow field in CDTD device (Ref. 3). The task of the modeling was to test how the rotational component of velocity will influence flow field.

In Figure 7, one of the geometries of the CDTD is shown with a computational grid covering the domain of integration. In Figure 8, the Iso-Mach lines for the geometry are shown for the inlet flow conditions indicated the figure 7.

The conclusions of preliminary research was that the program models the flow correctly and that, for the tested conditions, the results are close to those given by the program developed by Hirsch as discussed in Ref. 4.

## 2.9 Modeling of the Flow in Detonation Engine.

The flow field in the projected combustion chamber of a detonation engine was simulated numerically using the Godunov code. The task of this research was to study the dynamics of the discharge of the high pressure gas after detonation. A number of configurations were tried. In Figure 9, an example of this type of simulation can be seen. Pressure in the detonation chamber drops from 15 atm to 0.55 atm in 0.00131 second. It was important to establish that time since it is one of the limitations on the detonation frequency. In this example, the ability of the program to simulate large gradients of pressure can be seen.

## 2.10 Development of the SELCO Method.

A new method for supersonic flow simulation was developed. A full description of the method, with illustrations of its application to the supersonic flow over the wedge, is given in Appendix D. This method demonstrates that inaccurate modeling of the oblique shock waves produced by the Godunov method is the result of the obliqueness of the shock wave with respect to the edges of the cells of the computational grid covering domain of integration. It was shown that only when the shock surface is parallel to the two opposite edges of the cell that the oblique shock can be accurately calculated.

A new method of the Local Cell Orientation, - SELCO, was proposed to allow local reorientation of the cells in the vicinity of the shock waves. The efficiency of the SELCO method was demonstrated for the simulation of the oblique shock waves in the supersonic flow over the wedge.

## 2.11 Grid Generation for CDTD Inlet.

For a given distribution of the pressure measurement ports on the CDTD blade surface, a computational grid was developed. Several variants of the CDTD geometry were implemented. However all grids which were generated proved to lead to large computational errors. This work was not continued due to time constraints on the project.

## 3. Conclusions

The principal findings of the program of code testing were as follows:

1. The code has a robust ability to analyse unsteady time dependent flows and provide qualitative information on complex shock patterns and pressure fields.

2. With attention to boundary conditions and particularly grid structure it is possible to reproduce analytical flow solutions with great accuracy.

3.  The solutions produced are sensitive to grid orientation. The grid must be re-orientated locally along shock or discontinuity planes.

4.  Care must be used in selecting the grid distribution on areas of rapid curvature change.

Despite the program sensitivity under certain conditions, with skilled use it can be most instructive in establishing wave and shock structures in complex flow situations. A significant example is the unsteady boundary of Section 2.1 where in it was possible to generate a minimum loss passage angle for a wave rotor device.

6

## References

1. Eidelman, S.; Colella, P. and Shreeve, R. P., "Application of the Godunov Method and Higher Order Extension of the Godunov Method to Cascade Flow Modeling, " AIAA-83-1941-CP, AIAA 6th Computational Fluid Dynamics Conference, July 13-15, Danvers, Massachusetts, 1983.

2. A. Verhoff and P. J. O'Neil, A Natural Formulation for Numerical Solution of Euler Equations, MCAIR 83 - 031, M$^c$Donnell Aircraft Company, 1983.

3. Erwin, J; Phillips R. L.; Schulz, H. D.; Shreeve, R. P., Development of a Centrifugal Diffusor Test Device (CDTD), Part I - Design and construction of Los Speed Aparatus Naval Postgraduate School; Monterey, California; 1984 NPS 67084-003PR.

4. Schulz, H. D., Development of a Centrifugal Diffusor Test Device (CDTD), Part II - Initial Measurements and Flow Analysis, Naval Postgraduate School; Monterey, California; 1984 NPS 67-84-004PR.
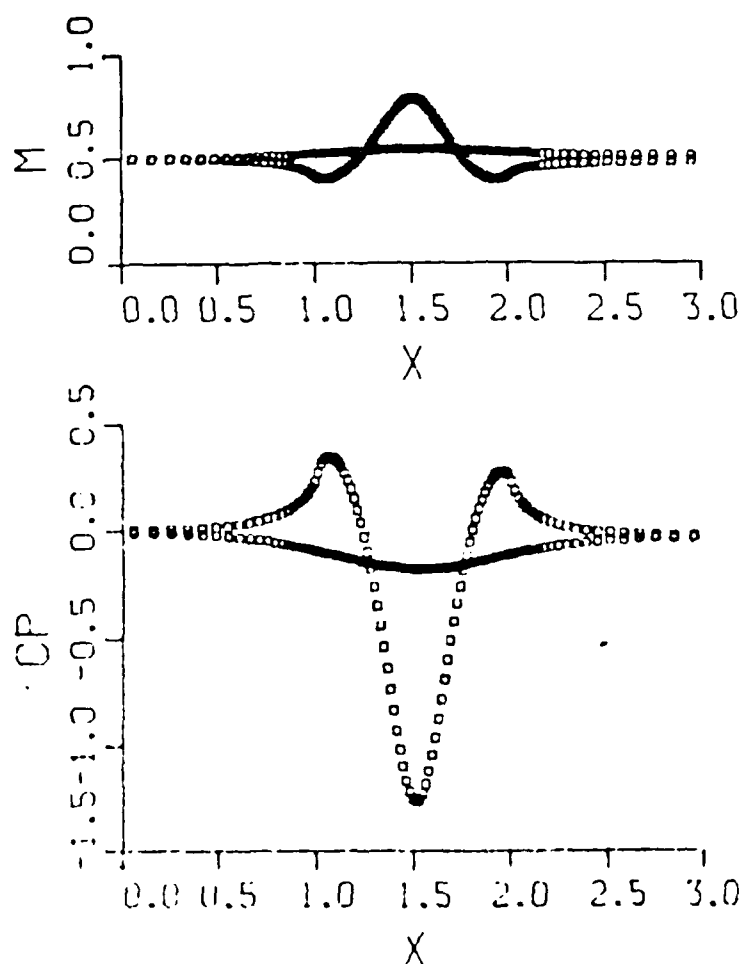
Figure 1. Pressure coefficient and surface Mach
number for the subsonic flow ($M_{in} = 0.5$)
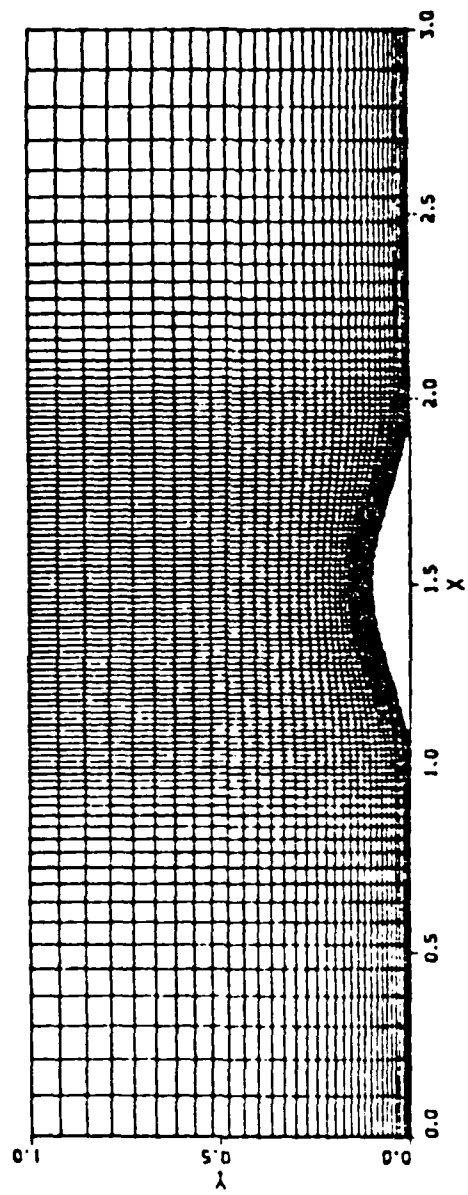in a channel with a sinusoidal arc bump.
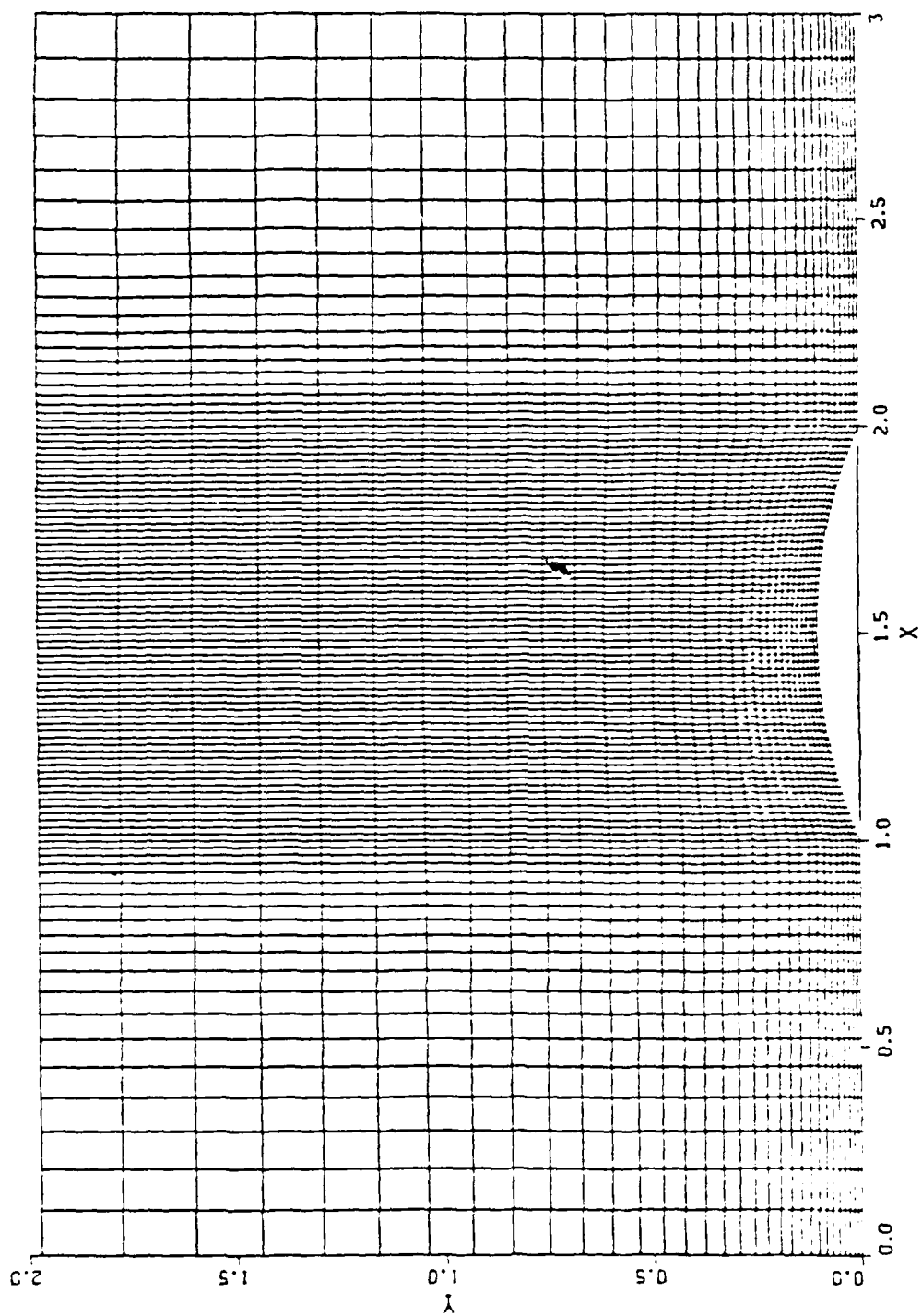
Figure 2. Grid for sinusoidal arc bump in a channel.
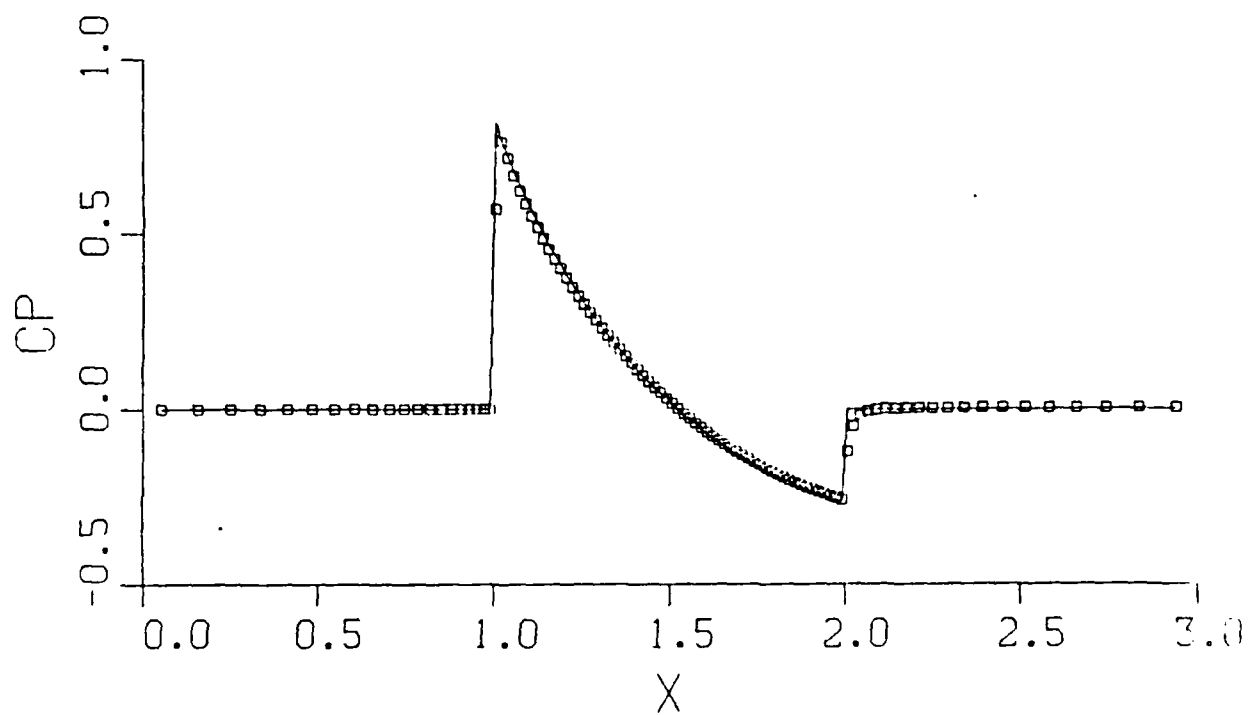
Figure 3. Grid for circular arc bump.

Figure 4.   Surface pressure coefficient.
(solid line = analytical
squares = numerical)

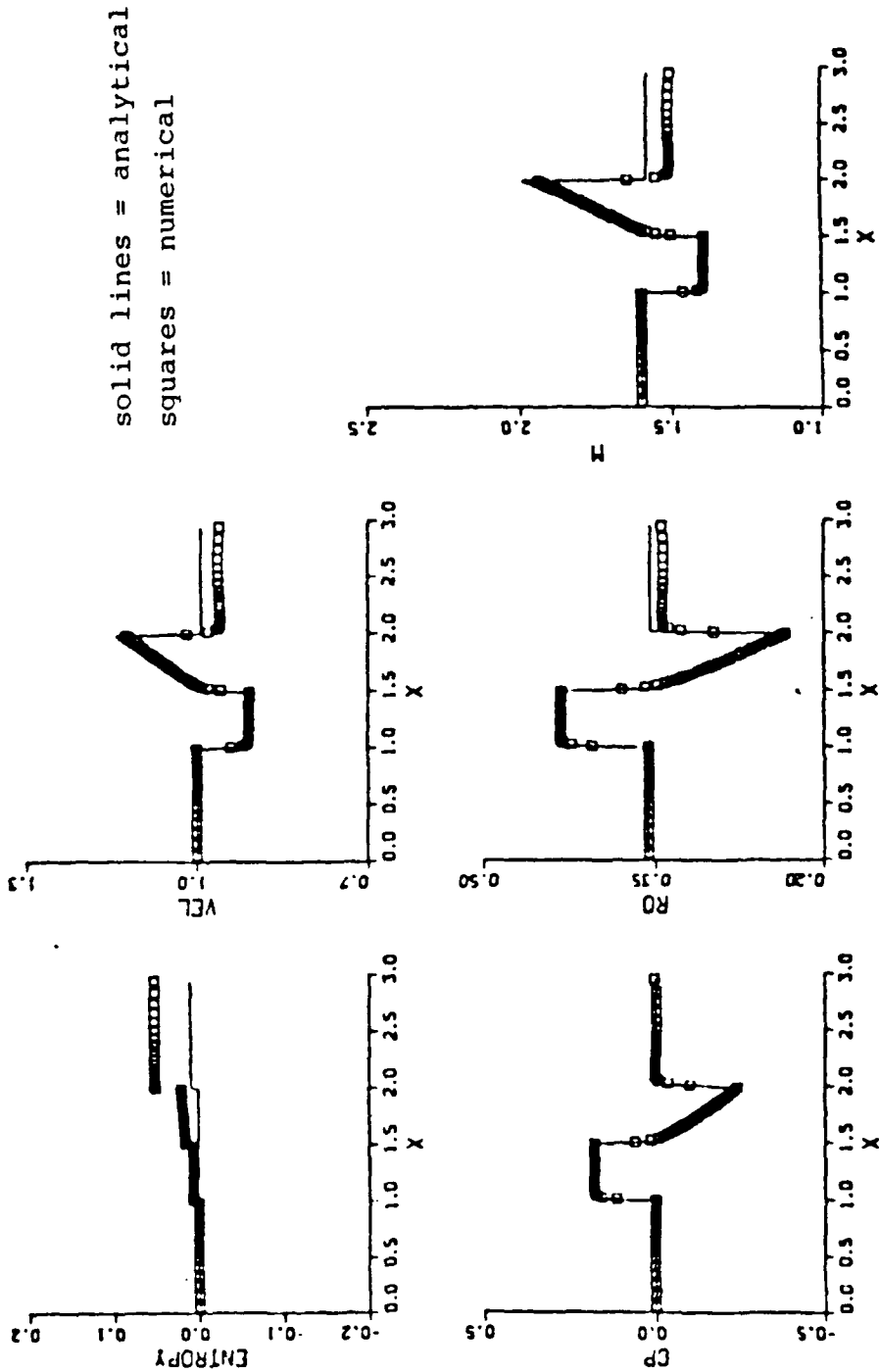solid lines = analytical
squares = numerical

Figure 5.   Surface pressure coefficients, entropy, density, velocity and
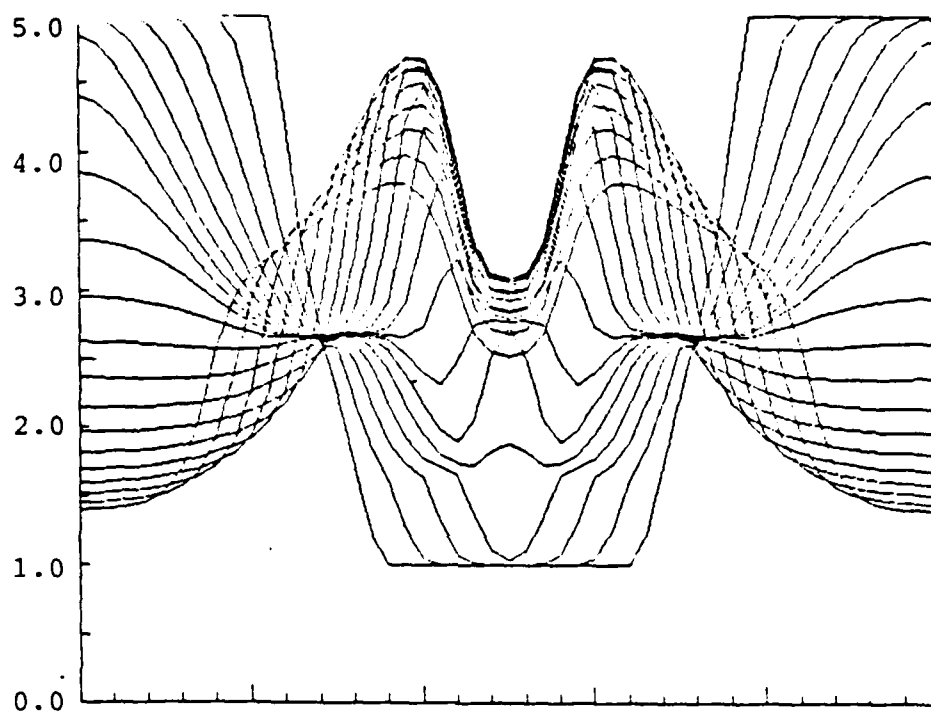Mach number for the flow in the channel at $M_\infty = 1.6$.

Figure 6.    1D shock tube with opposing diaphragms
density plots in time.

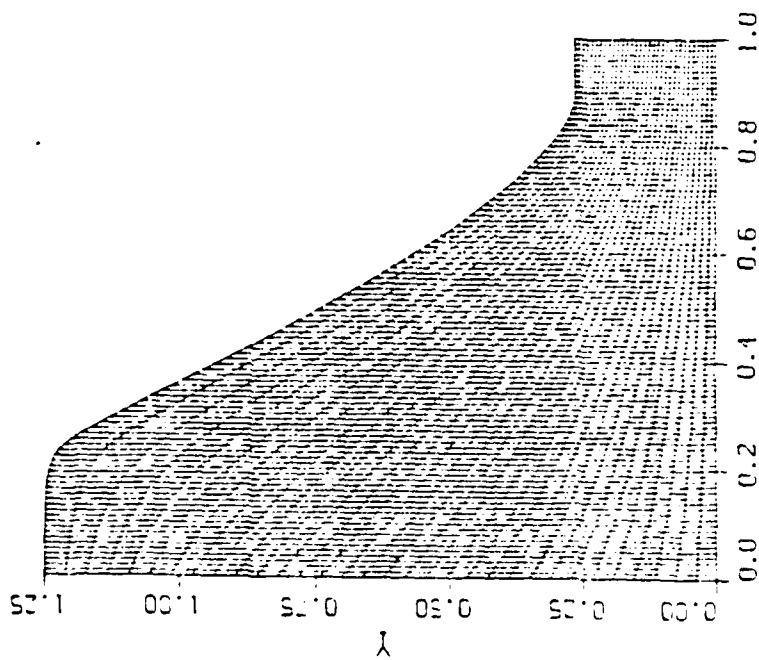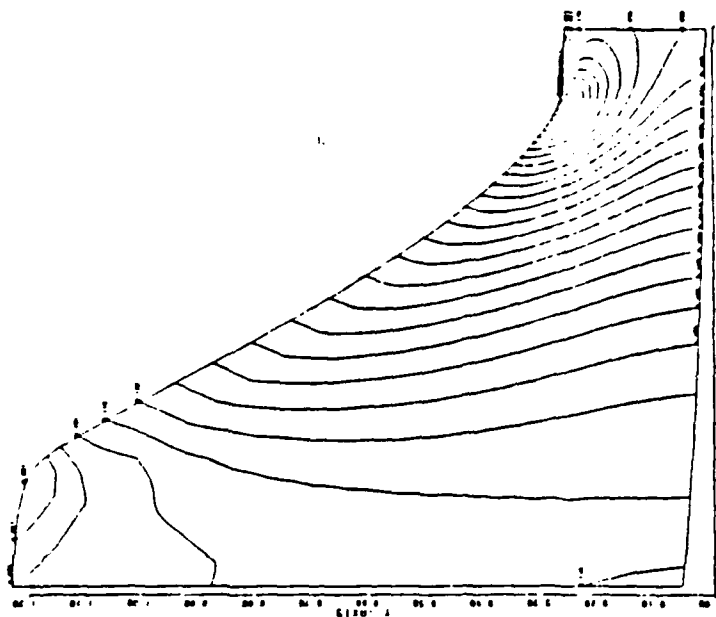Figure 8. Isomach lines ($U_{in} = 0.12$, $\omega = 1.1$)



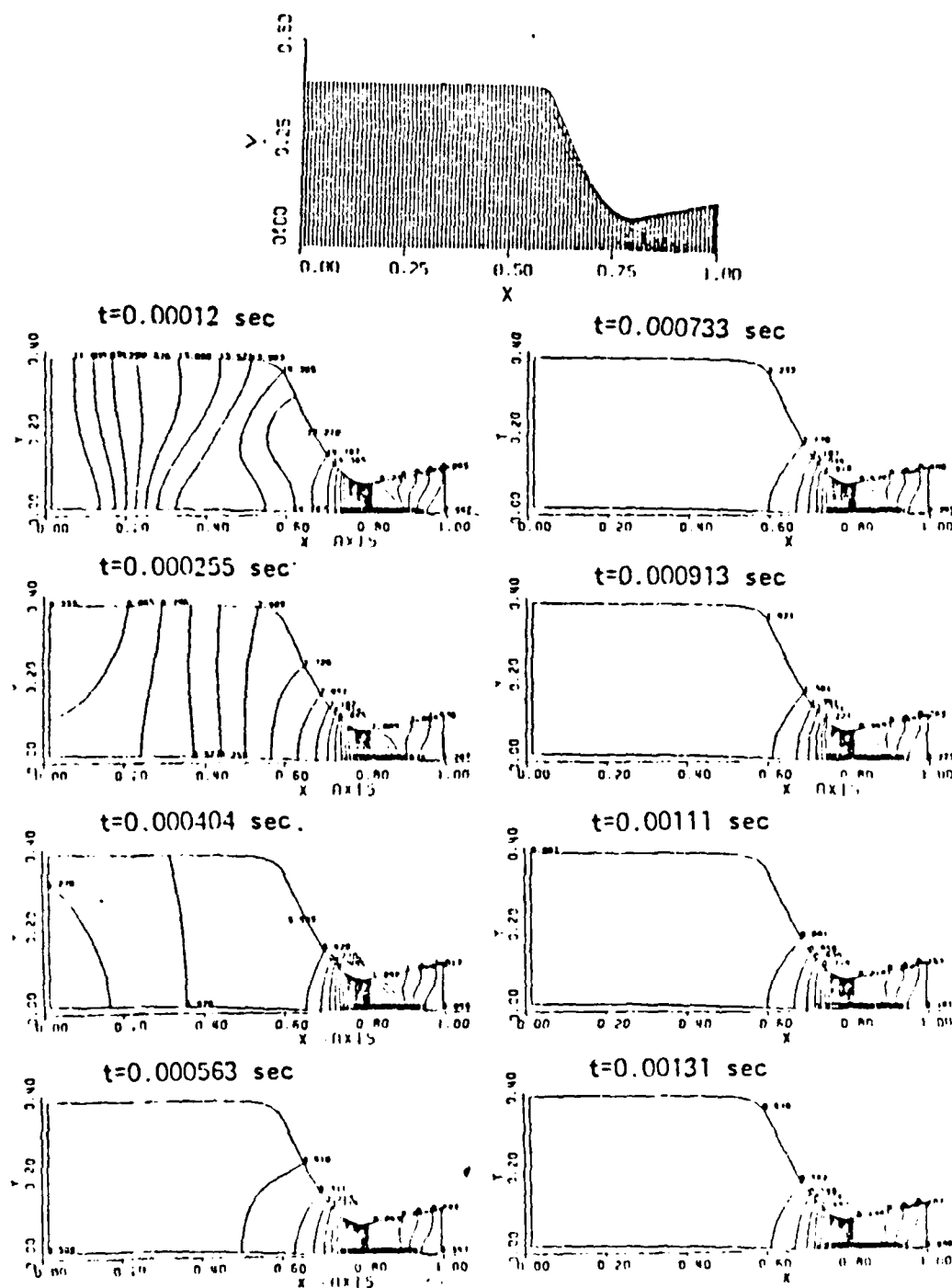Figure 7. Computational grid.

Figure 9.  Detonation engine analysis.

APPENDIX A

The Problem of Gradual Opening in Wave Rotor Passages Gradual Opening of
Skewed Passages in Wave Rotors.

# The Problem of Gradual Opening in Wave Rotor Passages

S. Eidelman*

*Naval Postgraduate School, Monterey, California*

The influence on the flow pattern of the gradual passage opening in the wave rotor is studied on the basis of numerical simulation. It is found that, in most cases, significant volume of the passage will have rotational flow, which should lead to the mixing between the driver and driven gases. In some cases, losses will occur also as a result of the multiple reflection of the shock and pressure waves from the passage walls. It is shown that the interface between driven and driver gas will be oblique to the passage walls, when the passage opens gradually, and the interface can retain its obliqueness to the walls.

## Introduction

WAVE rotors are devices that use wave propagation through the fluid in a rotor passage to transfer energy from one fluid to another[1] or to transfer energy from one fluid to rotor shaft and another fluid.[2] Wave rotors, wave engines, wave pressure exchangers, wave equalizers, and Comprex[1] are all based on the same idea of energy exchange in the unsteady waves, and the topic of the present study is relevant to all of these devices.

Wave rotors offer the potential for significant improvements in air-breathing engine propulsion cycles because they can be self-cooling, since both high-pressure gas and cold low-pressure gas use the same passage for alternate periods of time in the cycle. Combining a wave rotor with conventional turbomachinery components shows promise of significant reduction in specific fuel consumption without weight or size penalties.

The principles of operation of wave rotor devices and their commerical applications can be found in Refs. 1-3. For completeness, the general scheme of a wave pressure exchanger will be described, as illustrated in Fig. 1. One gas (driver) at high pressure is used to compress a second gas (driven). The process is arranged to occur in tube-like passages with trapezoidal cross section located on the periphery of a rotating drum or rotor. The compression is achieved successively in each rotor passage by means of compression waves or shock waves generated by the entering driver gas. The compressed driven gas is drawn off from the end of the passage when it aligns with an outlet port. The driver gas then undergoes a series of expansions to a lower pressure and is scavenged out by freshly inducted driven gas at approximately the same pressure level. This fresh "charge" is then compressed by the high-pressure driver gas and the cycle repeats itself. Steady rotation of the drum sequences the ends of the passages past stationary inlet ports, outlet ports, and endwalls. This establishes unsteady but periodic flow processes within the rotating passages and essentially steady flow in the inlet and outlet ports. The passage may be oriented axially as in Fig. 1 or at a stagger angle. In general, wave machines used as pure pressure exchangers (e.g., "Comprex") have usually axially oriented passages, while those with staggered passages may drive a shaft, since shaft work extraction is possible with this latter configuration.

In the design of the wave rotor, it is very desirable to determine the optimal ratio between the width and length of the single passage of the rotor. Usually only two parameters are evaluated to determine this ratio: skin friction losses and bypass losses. The number of passages on the rotor should be minimal to minimize skin friction losses. On the other hand, the passage should be narrow compared to the port widths to reduce flow bypass between inlet or outlet ports. The transient process of the passage opening or closing (as the passage end moves across a port or moves from a port to be closed by the endwall, respectively) usually is not considered in the design. It is generally assumed that the passage opening or closure occurs instantaneously.

Pearson[2] tried to take into account the gradual opening of the passage, assuming that the air in the passage is compressed in a series (usually three) of discrete compression waves which converge and ultimately merge to form a shock wave. This allowed him to design a complicated wave machine cycle for a rotor using relatively short passages. However, since the technique was one-dimensional it could not reveal the peculiarities of this essentially two-dimensional flow and would be valid only for very weak waves.

In the present study, by means of numerical modeling, we will examine in real-time how the gradual opening influences the wave formation in the wave rotor passages and how that should affect the rotor design.

## Model

The assumptions involved in the numerical simulations are described as follows.

The flow in each passage of the wave rotor is unsteady and periodic. At the same time, the flow through the port is (ideally) steady.[1,2] The peripheral width of the port is usually equal to several widths of a single passage, and herein it is assumed that the flow in the inlet or outlet port remains stationary when the passage-end encounters the port. For this reason the region of the port is not included in the computational domain shown in Fig. 2.

The time-dependent process of the passage-end translating across the region of the inlet or outlet port will be referred as the "gradual opening" of the passage. The passage opening process will be referred as "instantaneous," when the assumption is made that the passage instantaneously opens to the port area and is subjected immediately to the steady flow conditions at the port.

It is assumed that the flow is inviscid and can be modeled by the Euler equations. The unsteady two-dimensional Euler equations can be written in conservation law form as

$$\frac{\partial U}{\partial t} + \frac{\partial F}{\partial X} + \frac{\partial G}{\partial Y} = 0$$

where

$$U = \begin{Bmatrix} \rho \\ \rho u \\ \rho v \\ e \end{Bmatrix} \quad F = \begin{Bmatrix} \rho u \\ p + \rho u^2 \\ \rho u v \\ (e+p)u \end{Bmatrix} \quad G = \begin{Bmatrix} \rho v \\ \rho u v \\ p + \rho v^2 \\ (e+p)v \end{Bmatrix}$$

(1)

Here $\rho$ is the density, $u$ and $v$ the velocity components in the $X$ and $Y$ coordinate directions, $p$ the pressure, and $\gamma$ the ratio of specific heats. The energy per unit of volume, $e$, is defined by

$$e = \rho \left( \epsilon + \frac{u^2 + v^2}{2} \right)$$

where $\epsilon = P/(\gamma - 1)\rho$ is the internal energy. We look for the solution of the system of equations represented by Eq. (1) in the computational domain shown in Fig. 2 in time $t$ with the following conditions at the domain boundaries: a) solid wall along segments 1-3 and 2-4, b) outflow along segment 3-4, and c) inlet along segment 1-2.

It is assumed that initially at time $t = 0$, the passage of the wave rotor is filled with stationary gas at ambient conditions. When instantaneous opening of the wave rotor passage was simulated, it was assumed that at time $t = 0$, the flow at the inlet 1-2 was equal to the steady flow in the port. When gradual opening of the passage was simulated, at time $t = 0$, the inlet was closed and solid wall boundary conditions were imposed at the inlet 1-2. Then, this boundary condition was gradually replaced by the flow condition at the inlet port. The length uncovered to the inlet port region, where the solid wall boundary conditions were replaced by the inlet port conditions, was determined using the elapsed time and the velocity of the passage relative to the inlet port.

The Godunov method was used to obtain a numerical solution of Eq. (1) with the described boundary and initial conditions. Details of the implementation of the method and boundary conditions are given in Ref. 4.

The flowfield was modeled for the rectangular passage with a width of 0.02 m and a length of 0.12 m. The grid covering the computational domain of the passage is shown in Fig. 2.

## Results and Discussion

The following initial conditions were assumed for the air initially in the passage:

$$P_0 = 1 \text{ atm} \quad \rho_0 = 1.2 \text{ kg/m}^3 \quad U_0 = 0 \quad V_0 = 0$$

The driver gas entering through the port at the left-hand end was assumed to have the following properties:

$$P_d = 1.8 \text{ atm} \quad \rho_d = 1.81 \text{ kg/m}^3 \quad U_d = 150 \text{ m/s} \quad V_d = 0$$

These conditions correspond to a practical situation in a wave rotor when a passage filled with a quiescent fresh charge of air at ambient conditions encounters an inlet port supplying hot, high-pressure driver gas.

If the assumption is made that the passage instantaneously opens and is subjected to the conditions of the inlet flow at the left boundary 1-2 (see Fig. 2), then a perfectly one-dimensional flow pattern should develop in the passage. The results of the modeling of these conditions are presented in the form of pressure contours at progressively larger time steps in Fig. 3. Time $t = 0$ corresponds to the moment when the passage opens. Instantaneous opening of the passage is seen in Fig. 3 to lead to an immediate formation of a shock wave and subsequent propagation in the passage from the left to the right. The flow conditions at the inlet port are matched to the parameters of the rarefaction wave which effectively will
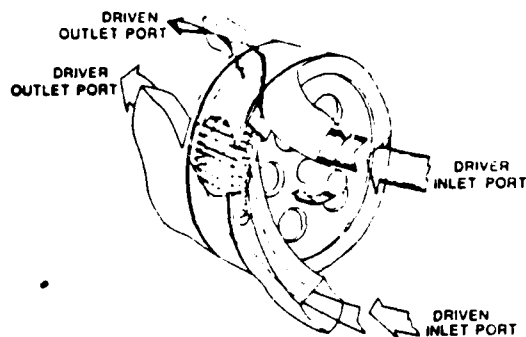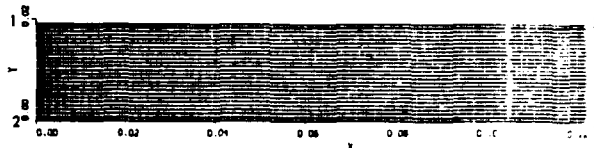


Fig. 1  Wave rotor operation scheme.
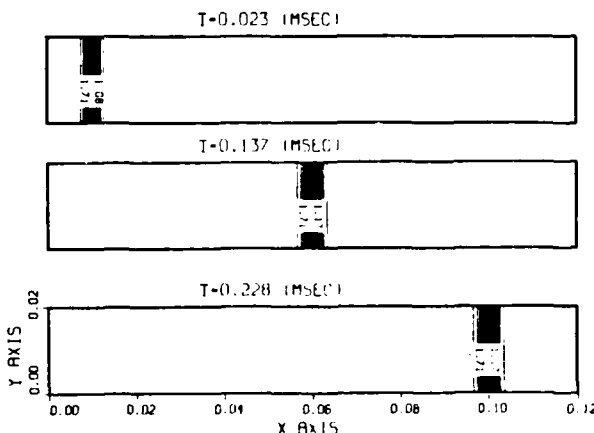


Fig. 2  Computational domain.



Fig. 3  Evolution in time of the shock wave formed after instantaneous passage opening.

cancel the rarefaction wave moving toward the inlet at the left end of the passage. For this reason the flow in the passage has no additional discontinuity. This situation is typical for a wave rotor, where flow conditions at the ports are chosen in such a way that waves do not propagate from the passages into inlet or outlet ports. The flow in the ports will therefore remain steady. In the case shown in Fig. 3, the shock wave was found to propagate with a velocity, $V_{sh} = 446$ m/s, the interface with a velocity $V_{in} = 150$ m/s, and all the parameters examined were confirmed accurately using one-dimensional gasdynamics relationships.

Most of the approaches used in wave rotor design are based on the assumption that the waves are one-dimensional in nature. When the gas is compressed by a weak shock wave, for instance, assumptions are made that, 1) the process is isoentropic, 2) the hot and cold gases are strictly separated by a planar interface, and 3) the flow is everywhere irrotational. This leads to the very high efficiencies projected for the compression. If the passage is wide enough so that viscous effects can be neglected, this model of the compression in the wave rotor passage is realistic, but only for instantaneous passage opening or for a very long passage. Results presented below illustrate how the gradual passage opening affects the compression process.

In Fig. 4, the pressure and Mach number contours in the passage are shown at a sequence of times for the case of a gradual opening to the inlet port with a velocity of 100 m/s. Parameters for the gas in the passage, before opening begins, and in the inlet port are the same as for the case of instantaneous opening. The dynamics of the flow development seen in Fig. 4a is very different from that shown in Fig. 3. First, curved pressure waves radiate from the initial small opening appearing at the lower corner of the inlet on the left side of the passage ($t = 0.044$ ms in Fig. 4). Subsequently, these waves reflect from the upper wall of the passage and at time $t = 0.125$ ms have formed a row of compression waves which have approximately straight fronts normal to the wall of the passage. Initially, compression waves of this kind occupy a small part of the region with disturbed gas. In the region well behind the front of this quasi-one-dimensional propagation, compression waves are curved and are the result of the interaction between the waves reflecting back and forth between the lower and upper walls of the passage and the new waves created by the progressive opening of the port to the passage. Since it is possible to see in Fig. 4 for the times $t = 0.084$ and 0.166 ms, respectively, the flow behind the quasi-one-dimensional region is highly rotational and is relatively constant pressure in the $X$ direction. The passage became fully opened only at $t = 0.2$ ms. At this time compression waves are propagating along the length of the passage and the pressure rises gradually from 1 atm at the right end to 1.8 atm at the left end. The front of converging compression waves will eventually become a shock wave, but this will occur at some later time and outside the computational domain.

It was concluded from the case presented in Fig. 4 that a passage length-to-width ratio of 6 will lead to very high mixing losses and nonuniform and inefficient compression, since in this case the region of rotational flow occupies half of the passage volume. Additional losses will be produced because of the highly rotational flow within each of the two gases.

In Fig. 5, pressure and velocity contours are shown for the case of gradual opening of the passage with a velocity of 200 m/s. Full opening of the passage in this case occurred at $t = 0.1$ ms. A curved shock wave is formed at $t = 0.044$ ms. This shock wave (see Fig. 5a) partially reflects from the upper wall of the passage and then, gradually converging with its main front, forms an almost planar shock front at the time $t = 0.252$ ms. However, even then the flow is highly rotational behind the shock front, and the region of rotational flow occupies one-third of the passage volume. In this region the gas velocity increases from $M = 0.3$ at the upper wall to $M = 0.52$ at the lower wall.

When the velocity of the passage opening is increased to 500 m/s (see Fig. 6) the passage becomes fully open at $t = 0.04$ ms. Because of the fast opening of the passage, the shock wave at the time $t = 0.04$ ms is less curved and only a small fraction of the shock front reflects from the upper wall. This reflected part of the shock front converges with the main front at $t = 0.172$ ms. From that time on, the flow pattern in the passage is mostly one-dimensional with a small and weakening region of rotational flow behind the main front. Nevertheless, even for this case, with passage length-passage width = 3, there will be very high mixing losses, with a large part of the passage volume subjected to rotational flow.

In order to study how the strength of the shock wave influences the flow pattern developing in the passage, an additional case was simulated where the parameters of the driver gas at the inlet port area were increased; namely, to

$$P_1 = 2.85 \text{ atm} \quad C_1 = 283 \text{ m/s} \quad \rho_1 = 4 \text{ kg/m}^3$$

As in the previous case, the parameters of the driver gas were chosen in such a way that waves do not propagate back into the port when the passage opens. Results of this simulation
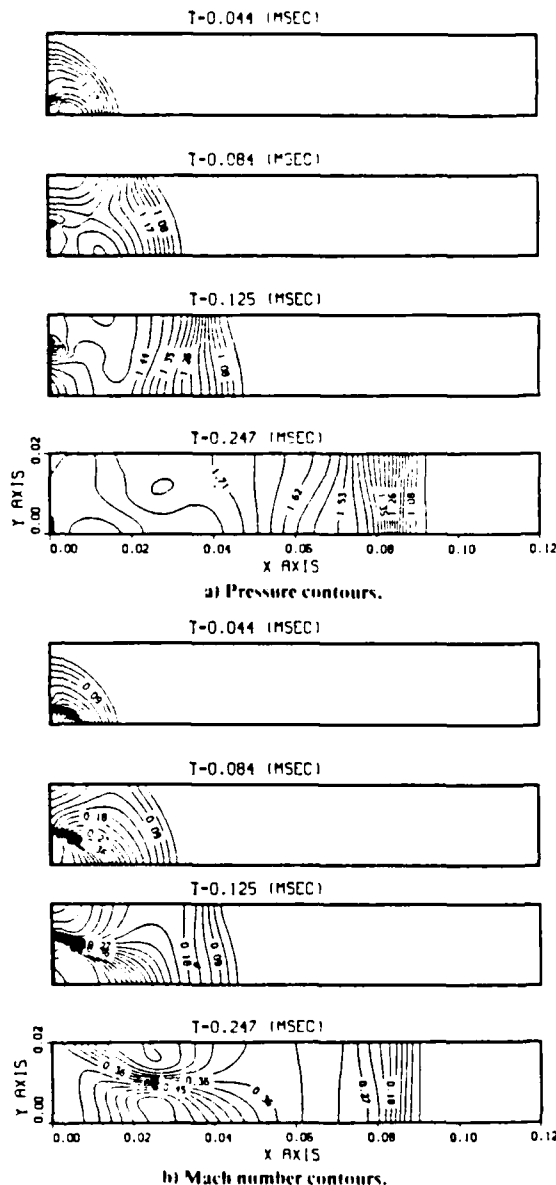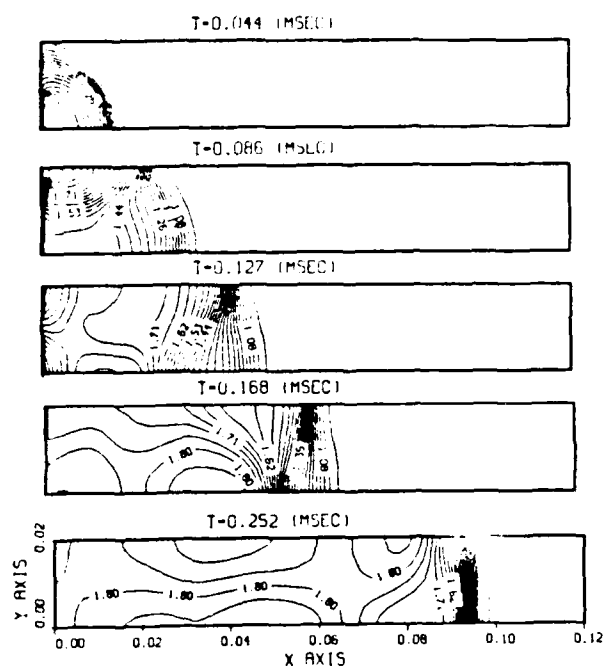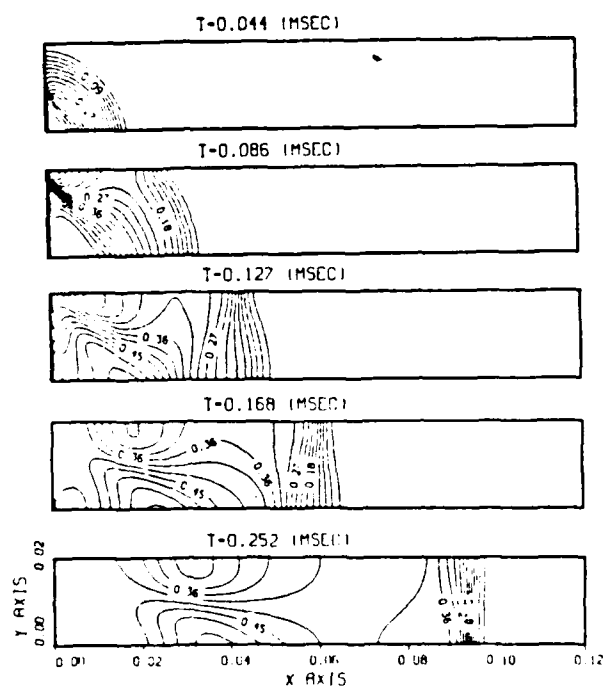


a) Pressure contours.



b) Mach number contours.

Fig. 4　Flow pattern evolution for the passage gradual opening with a velocity of 100 m/s.

are shown in Fig. 7. The velocity of the passage opening was $V = 250$ m/s. It was concluded from the results presented in Fig. 7 that an increase in the initial shock strength leads to stronger reflections and substantial increases in the flow rotation. This, in turn, will lead to increased losses because of mixing of the driver and driven gases. The pattern of multiple reflections of the shock wave from the upper and lower walls of the passage can be seen in Fig. 7a. At time $t = 0.073$ ms the shock wave reflected from the upper wall is propagating toward the lower wall. Part of the reflected shock wave front converges with the main shock wave, and part begins to reflect from the lower wall ($t = 0.109$ ms). The multiple reflection weakens the reflected shock, but the reflection between the walls of the passage continues and can be followed for $t = 0.211$ and 0.245 ms. It is clear that for these conditions even passages with a length-to-width ratio of 6 will have substantial mixing losses because of the rotational flow.

A different situation is found for the passage opening to the inlet port of the driven gas. At this port, the pressure and velocity of the (driver) gas in the passage should be matched with the pressure and velocity of the (driven) gas at the inlet
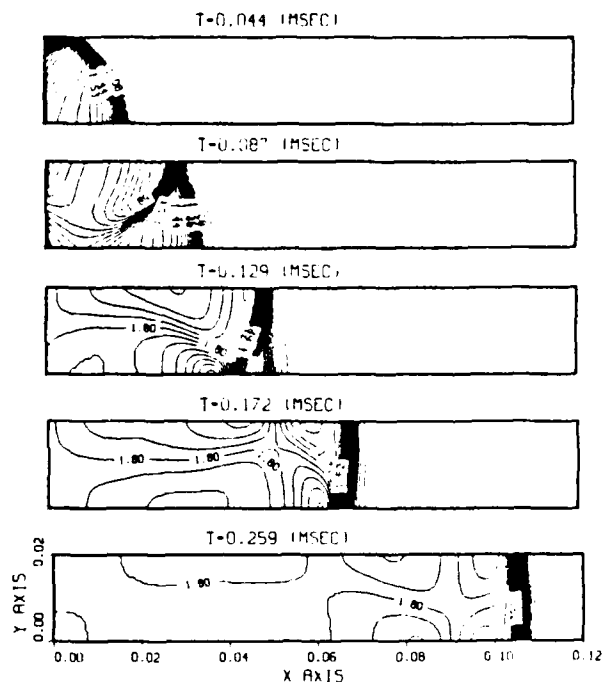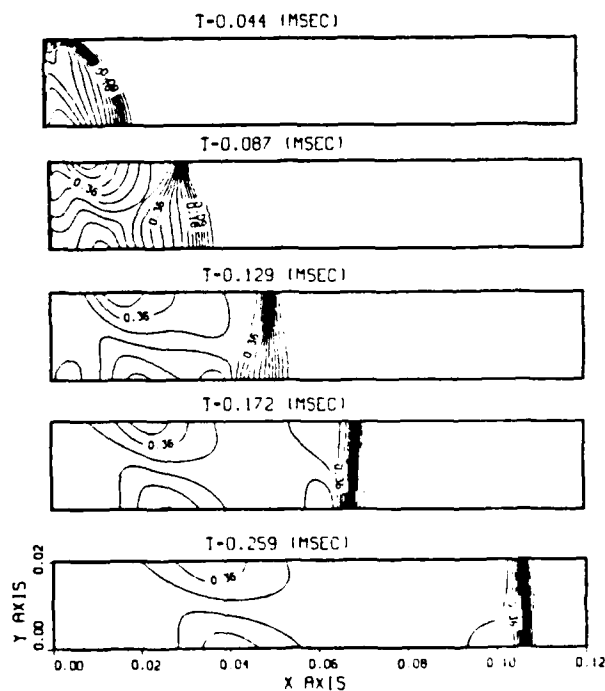
a) Pressure contours.



b) Mach number contours.

Fig. 5  Flow pattern evolution for the passage gradual opening with a velocity of 200 m/s.



a) Pressure contours.



b) Mach number contours.

Fig. 6  Flow pattern evolution for the passage gradual opening with a velocity of 500 m/s.

If the passage opens instantaneously, the flowfield in the passage will have only one discontinuity—the interface between the fresh air and exhaust gas entering and leaving the passage, respectively. To model this condition for the gradual passage opening, it was assumed that in the passage, $P = 1$ atm, $\rho = 0.5$ kg/m³, $U_x = 150$ m/s, and $U_y = 0$; in the port, $P = 1$ atm, $\rho_a = 1.4$ kg/m³, $U_x = 150$ m/s, and $U_y = 0$. The velocity of the passage opening was $V = 200$ m/s.

Results for this simulation are presented in Fig. 8. It can be seen that, since at first moment most of the inlet cross section

is blocked by the wall, a rarefaction wave reflects from the inlet wall. The passage full opening occurs at $t = 0.1$ ms. From this time on the pressure deviation in the flowfield weakens and at $t = 0.22$ ms the pressure is almost completely uniform and equal to the static pressure in both the undisturbed fresh air and exhaust gas. Figure 8b shows that the interface will carry the imprint of the gradual passage opening a long time after the passage becomes fully open. There is no dissipative mechanism included in the mathematical model used in this study to force the interface to become normal to the passage
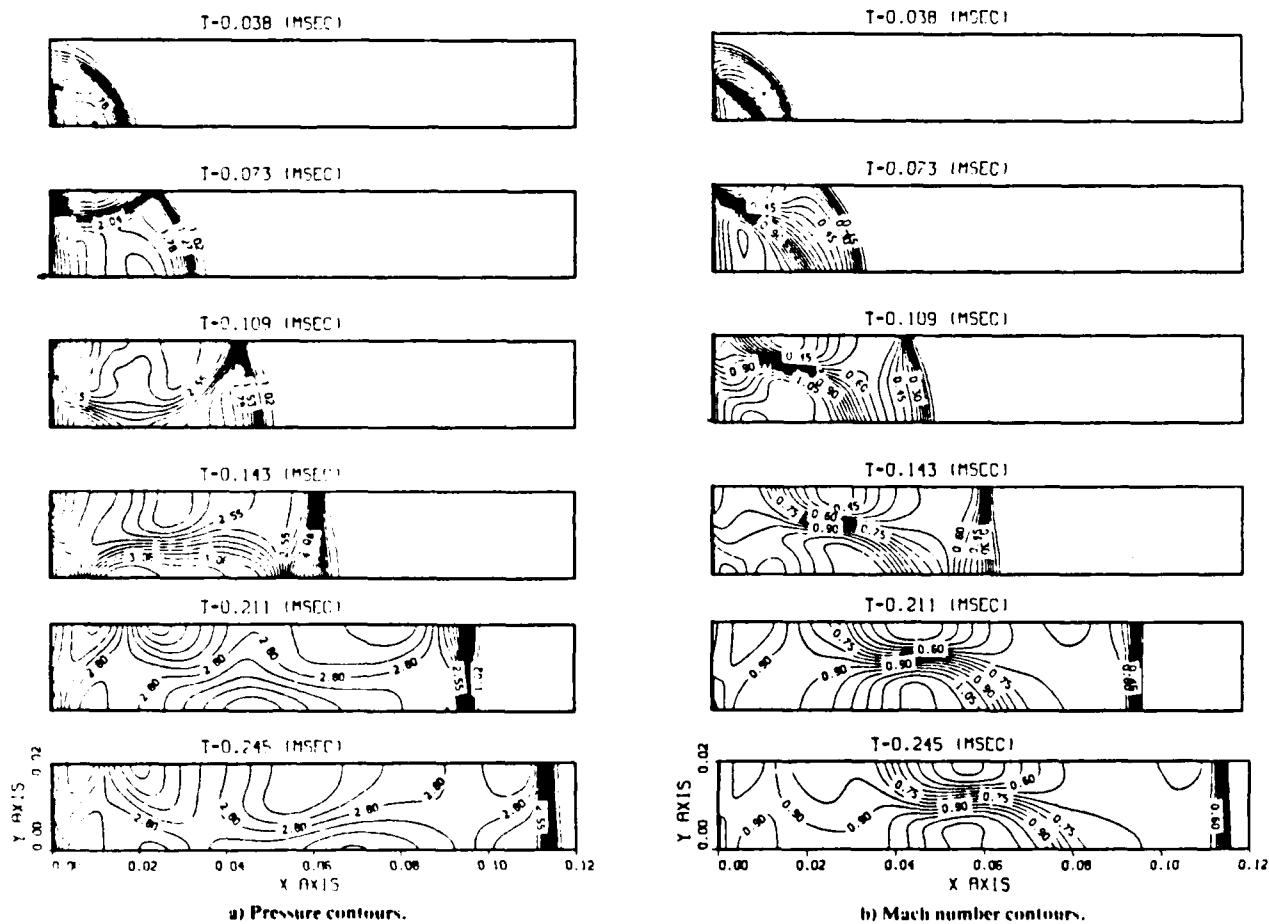
a) Pressure contours.

b) Mach number contours.

Fig. 7   Flow pattern evolution for the gas with higher total enthalpy at the inlet port.

a) Pressure contours.

Fig. 8   Evolution of the interface.

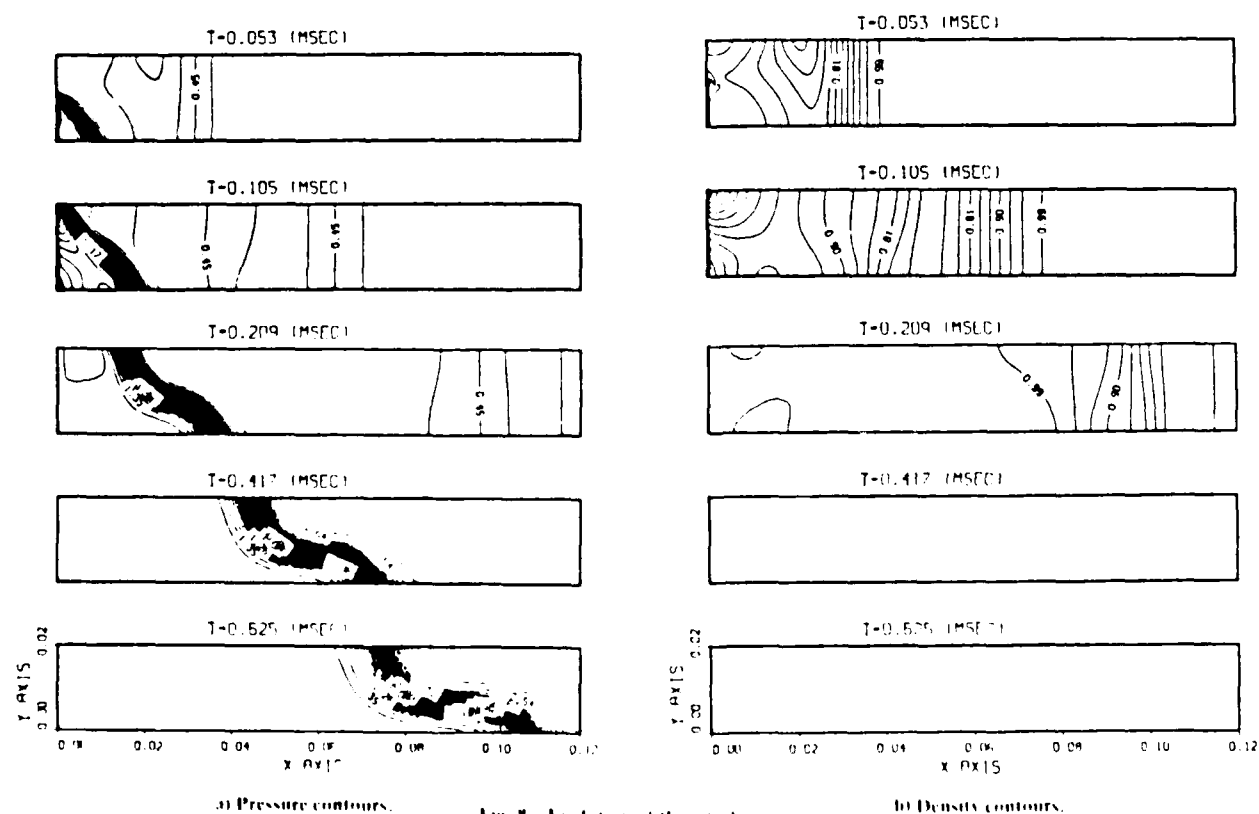b) Density contours.

walls. Therefore, the interface will "remember" the dynamics of the gradual passage opening in passages with large length-to-width ratio.

## Conclusions

It is shown in the present study, on the basis of numerical modeling, that the dynamics of the passage opening significantly affects the flow pattern in the passages of wave rotor devices. For rectangular axial passages, even when the velocity of the passage opening is constant, a one-dimensional flow pattern forms only in passages with a length-to-width ratio larger than 3. In the region preceding the formation of the one-dimensional flow pattern, the flow is rotational and, in some instances, contains shock and pressure waves which repetitively reflect from the upper and lower walls of the passage. In practice this would lead to significant mixing between the driver gas (e.g., exhaust gas) and driven gas (e.g., fresh air) and reduce the efficiency of the engine cycle. With a reduction in the velocity of the passage opening, the volume of the mixing region increases as a result of the rotational flow which develops from the slow opening of the passage. With an increase in shock wave strength, the volume of the mixing region increases as a result of the rotational flow which develops form multiple reflections of the shock and pressure waves from the passage walls.

Numerical modeling of the process of gradual passage opening at the inlet port of the driven gas revealed that the interface between the gases will move all the way through the passage with a frozen pattern of distortion or obliqueness to the passage walls. The interface obliqueness increases when the velocity of the passage opening decreases.

In all, it can be concluded that taking into account the gradual passage opening is essential for the wave machine design, not only for proper timing and wave arrangement but also because of the losses which will occur due to mixing and wave reflections. The gap between projected and achieved efficiencies of wave machines[6,7] could be partially due to neglect of the effects of the gradual passage opening which are studied herein.

## References

[1]Croes, N. "The Principle of the Pressure-Wave Machine as Used for Charging Diesel Engines," Department of Comprex Research, A. G. Brown Boveri and Cie, Baden, Switzerland

[2]Pearson, R. D., "Pressure Exchangers and Pressure Exchange Engines," *Thermodynamics and Gas Dynamics of Internal Combustion Engines*, compiled by D. E. Winterbone and S. C. Low, Chap. 16.

[3]Thayer III, W. J., Taussing, R. T., Zumdieck, J. F., Vaidyanathan, T. S., and Christiansen, W. H., "Energy Exchanger Performance and Power Cycle Evaluation-Experiment and Analysis," DOE AC06-78E-R01084, April 1981.

[4]Eidelman, S., Colella, P., and Shreeve, R. P., "Application of the Godunov Method and Its Second-Order Extension to Cascade Flow Modeling," AIAA Journal, Vol. 22, 11, P. 1609, 1984

[5]Shreeve, R. P., Mathur, A., Eidelman, S., and Erwin, J., "Wave Rotor Technology Status and Research Progress Report," Naval Postgraduate School, Monterey, Calif., NPS67-82-014PR, Nov. 1982.

[6]Coleman, R. C. and Weber, H. E., "Integral Turbo-Compressor Wave Engine," U. S. Patent 3,811,796, 1976

[7]"Exploratory and Advanced Development Programs," Naval Air Propulsion Center, Trenton, N. J., NADC-1-83, April 1983

Gradual Opening of Skewed Passages in Wave Rotors

## Introduction

The problem of gradual opening of rectangular axial passage in wave
rotors was studied in our article[1] published in the January issue of Journal
of Propulsion and Power. There we have defined the problem of gradual
opening in the wave rotor passage and the mathematical model which was used
to simulate the opening process. In this article we will assume that the
reader is familiar with the reference[1], and it could be regarded as an
extension to the that reference.

If the wave rotor is used to produce shaft power, it's passages should
be skewed in one form or another. In this paper we will analyze the gradual
opening of a skewed passage and will examine the conclusion drawn for the
rectangular axial passage for this more general geometry of the passage.

## Results and Discussion

The main conclusion of the study on gradual opening of rectangular
passage is that in order to minimize the mixing losses caused by rotational
flow in the passage, the opening velocity should be very high. In the
limit, instantaneous opening of the wave rotor passage will lead to one

dimentional flow pattern in the passage will have minimal mixing losses.
When the passage of the wave rotor is skewed, even instantaneous opening of
the passage will not lead to development of the one dimensional flow pattern
with small mixing losses. That statement will be demonstrated in the
following example.

Let's model the opening process for the passage 0.02 m wide and 0.24 m
long. It has left and right hand inlets parallel to the y-axis and upper
and lower walls of the passage form $60^0$ angle with positive direction of the
x-axis. It is assumed that initially air in the passage is at the following
conditions.

$$P_o = 1 \text{ atm}; \ \rho_o = 1.2 \text{ kg/M}^3; \ U_o = 0; \ V_o = 0$$

The driver gas entering through the port at the left hand end was assumed to
have the following properties:

$$P_d = 1.8 \text{ atm}; \ \rho_d = 1.81 \text{ kg/M}^3; \ U_d = 75 \text{ M/sec}; \ V_d = 129.9 \text{ M/sec}$$

The conditions for the driver and driven gas are the same as in case of the
rectangular passage which we reported in the previous paragraph.

In Figures 1a and 1b results for simulation of the instantaneous
opening of the skewed passage are shown in form of pressure and velocity
contours at the sequences of times. The flow pattern near the inlet in
Figure 1 is highly rotational which suggests very high mixing losses. That
is caused partially by reorientation of the shock wave. At the first

moments of time after the opening of the passage the shock wave between the driven and driver gases is oblique to the lower and upper walls of the passage. At later times this shock wave turns and becomes normal to the upper and lower walls. Thus, incontrast with rectangular for skewed geometry passages there is no obvious condition for minimizing the mixing losses caused by the inlet opening.

Let's find the conditions for opening of the skewed passage which will lead to minimal mixing between driver and driven gases. As we have stated before, rotational flow in the instantaneously opened skewed passage, will develop because of the rotation of the shock wave from the parallel position to the inlet (initially) to the position where it is normal to the upper and lower walls of the passage (when the flow is developed). If we could form a shock wave which will be all the time normal to the lower and upper passage walls then the rotational flow and mixing will be minimal.

Analysing the formation of the shock wave front at the inlet we concluded that for the shock wave forming at the inlet to remain normal to the lower wall, inlet should be opening at the rate:

$$V_{op} = V_{sh} /\sin \alpha_{sk} \qquad (1)$$

where $V_{op}$ – velocity of the inlet opening.

$V_{sh}$ – shock wave velocity in the media.

$\alpha_{sk}$ – angle of the skewed passage.

The velocity is equal to the velocity with which the shock wave surface will slide along the inlets wall.

In Figs. 2a and 2b results for the modeling of the gradual opening of the skewed passage inlet with the opening velocity in accordance to equation

(2) are shown. As it is obvious from coutour plots of pressure and velocity
in Figs. 2a and 2b, opening the passage with velocity $V_{op}$ calculated from
equation (1) assures development of the flow pattern with minimal mixing.
The shock wave surface in that case remains at all times normal to the walls
of the passage.

## Conclusions

Modeling of the gradual opening of the skewed passage revealed the way
to minimize mixing losses at the passage inlet. The mixing will be minimal
when the velocity of the opening is matched with shock wave velocity in the
passage divided by the angle of skewed passage. Our simulations shows that
even when conditions for the optimal opening are not satisfied exactly,
reduction of the rotational mixing could be significant if the opening
velocity is $\pm15\%$ of the optimal value.

We can also conclude that a very high opening velocity is required in
order to obtain low mixing loss. The opening velocity of the passage should
be always higher than the velocity of the shock wave generated in the wave
rotor passage at the high pressure inlet. Even substantially skewed passage
will require the opening speed ~10% higher than the shock wave velocity in
the passage which is not easy to achieve for the typical flow conditions in
the wave rotor.

Another limitation is that even when this optimal speed of opening is
achieved at one port, it will not be optimal at other ports; so,
optimization will not be full. However, mixing losses in the skewed
passages will be smaller than in rectangular one, if the gradual opening of
the skewed passage begins from its acute angle.

## Acknowledgment

## References

1. Eidelman S., "The Problem of Gradual Opening in Wave Rotor Passages", Jour. of Propulsion and Power, Vol.1, pp. 23-28, 1985.
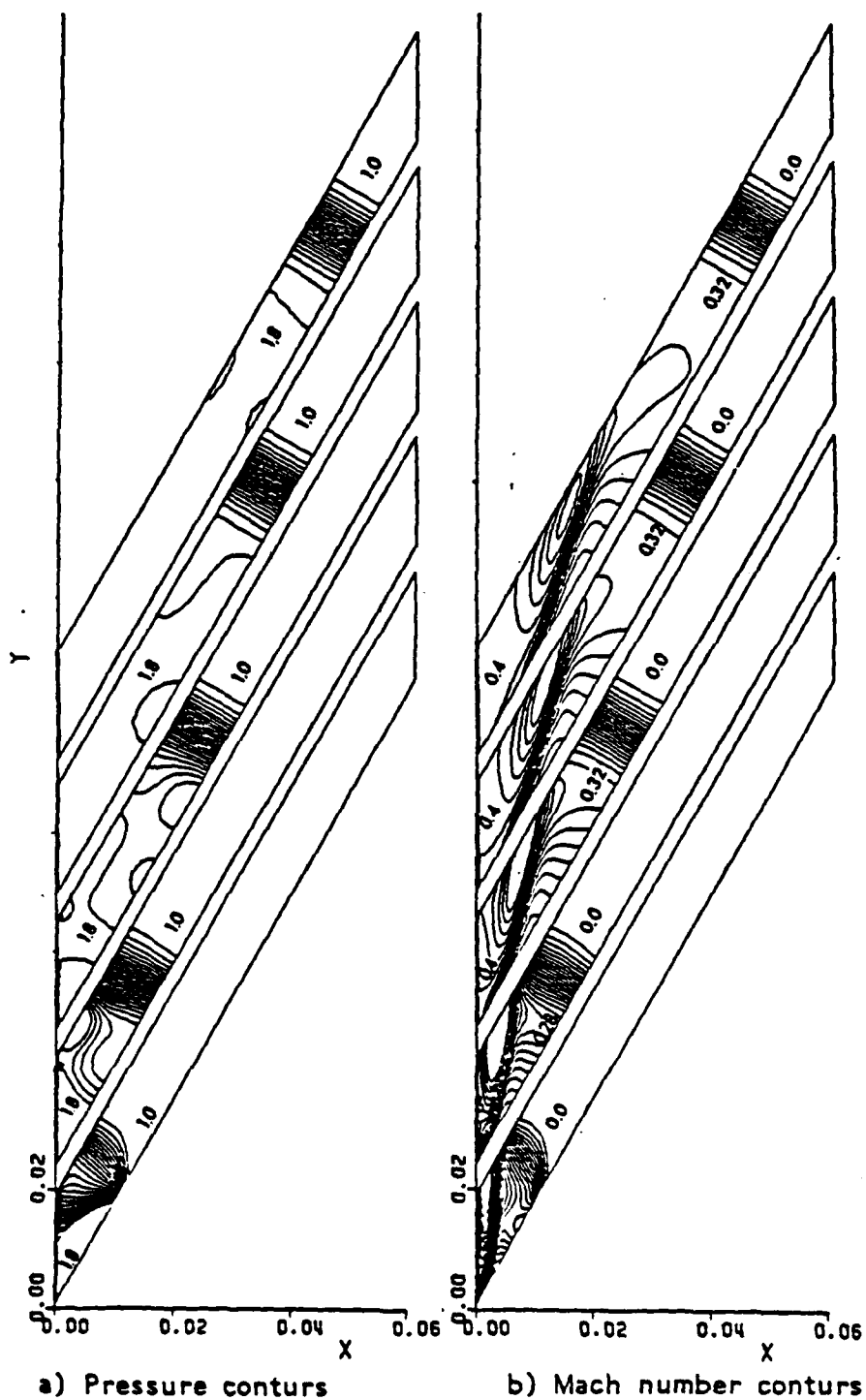
a) Pressure conturs      b) Mach number conturs

Figure 1    The flow pattern evolution after instantaneous
opening of the 60° skewed passage.
Time is along the Y - axis (no to scale).

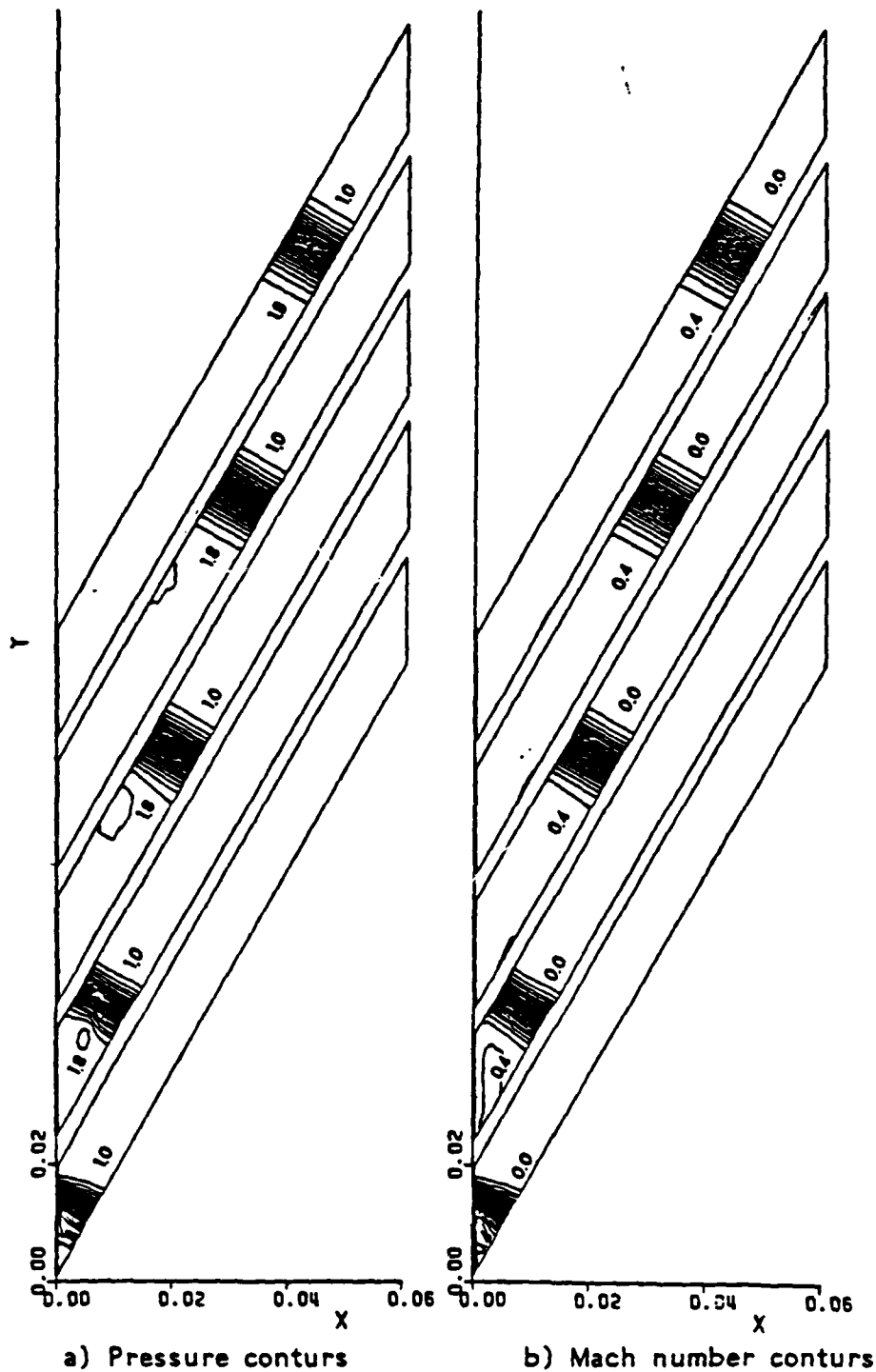a) Pressure conturs                    b) Mach number conturs

Figure 2   The flow pattern evolution for the passage gradual
           opening with the velocity according to $V_{OPEN} = V_{SH}/SIN\alpha_{SK}$
           Time is along the Y - axis (no to scale).

APPENDIX B

Numerical Modeling of the Non-Steady Thrust Produced by Intermittent Pressure
Rise in a Diverging Channel.

Numerical Modeling of the Nonsteady Thrust Produced by

Intermittent Pressure Rise in a Diverging Channel

by

Shmuel Eidelman* and Raymond P. Shreeve**


Turbopropulsion Laboratory
Naval Postgraduate School
Monterey, California 93943

* Adjunct Research Professor, Department of Aeronautics
** Director, Turbopropulsion Laboratory, and Adjunct Professor, Department of
Aeronautics

## ABSTRACT

The dynamics of the expansion of detonation products in a diverging channel were investigated numerically. A two-dimensional unsteady Euler code based on the Godunov method was employed. The influences of particular features in the expansion process, such as the presence of reversed flow and propagation of hammer shocks, on the production of thrust were examined. Sequentially expansions of detonation products were also modeled and it was concluded that in order to maintain a high frequency periodic mode of operation for propulsion applications the channel should be refilled with ambient air after each expansion. The influence of the ratio of ambient air to detonation product volume on the dynamics of the thrust production, and on the impulse generated during the expansion, are also reported.

## NOMENCLATURE

$dA_x$   – element of channel internal surface area normal to the x-axis
$e$   – energy per unit volume
$p$   – pressure
$t$   – time
$u$   – component of velocity in x direction
$v$   – component of velocity in y direction
$x$   – cartesian coordinate
$y$   – cartesian coordinate
$\varepsilon$   – internal energy per unit mass
$\gamma$   – ratio of specific heats
$\rho$   – density
subscripts
$0$   – conditions at t=0 in combustion products
$ex$   – external
$L$   – along inner wall of the channel

## INTRODUCTION

Early in the development of propulsion engines for aircraft, a choice had to be made between engine concepts based on nonsteady or on steady gasdynamic

processes. Concepts based on steady gasdynamic processes were pursued largely because they were simpler to analyze and to appreciate conceptually. On the basis of the chosen steady concepts, engines were built, developed and perfected with time. The nonsteady concepts, which looked as promising initially, were not developed and remain today in the conceptual stage.

The need for a more thermally efficient small engines for various military and civilian applications, has led, at intervals, to a reexamination of nonsteady concepts (1,2,3). Today, such an examination can be made more thoroughly. For, while nonsteady engine concepts were at one time extremely difficult to analyze, numerical modeling on computers can now provide time-dependent pictures of internal flow processes. This can provide efficient tools for preliminary design calculations and eventually analysis tools for design optimization.

From the late 50's until the early 70's, the feasibility of an engine operating with intermittent detonative combustion was studied at the University of Michigan (4,5,6). Specific impulses over 2100 sec. were realized for a single linear shock tube operating intermittently with frequencies up to 35 detonations per second. Nicholls et al. showed that an engine operating intermittently on detonation waves will have some advantages over an engine operating on deflagration. In general, it will have very high specific thrust. The engine will be very simple mechanically, and not require precompression of the mixture for efficient combustion.

One of the disadvantages of the engine is that jet velocities developed after detonative combustion are very high. Efficient operation of the engine for propulsion could be realized only at high supersonic vehicle velocities (Mach number of about 4). In order to reduce the velocity of the out-coming jet, it was proposed to use spinning detonation (6). But the spinning detonation process proved to be unsuitable for use in an engine because it was unstable. Back et al. (8) studied the feasibility of using detonative

propulsion in Jupiter's atmosphere, and obtained a
number of results for various types of nozzles.

Motivated by the potential applications, of
detonative propulsion, in the present study the
process of the expansion of detonation products in a
diverging channel or diffuser of a detonation engine
were modeled numerically. The model and computer
program were then applied to calculate repetitive
firing, and the effect of changing the diffuser
length.

THE MATHEMATICAL MODEL AND NUMERICAL SOLUTION

It is assumed that the jet-propulsion nozzles of
an engine using detonative combustion can be
constructed from a number of straight diverging
channels which are grouped, or clustered together. In
one cycle of the engine, a small volume of each tube
is filled with the combustible mixture and undergoes
detonation. Then the detonation products expand into
the stationary gas which fills the rest of the tube at
ambient pressure and temperature. The tube is
diverging and so the shock wave decays in strength.
Finally, a weak shock wave leaves the tube, and a
subsonic flow of gas discharges from the exit of the
channel.

It is assumed that the flow is periodic along the
lines which are a continuation of the walls of the
channel. This implies that we are modeling the flow
in a centrally located channel of the cluster.

It is further assumed that the flow is inviscid.

The unsteady two-dimensional Euler equations can
be written in conservation law form as:

$$\frac{\partial U}{\partial t} + \frac{\partial F}{\partial X} + \frac{\partial G}{\partial Y} = 0$$

where

$$U = \begin{bmatrix} \rho \\ \rho u \\ \rho v \\ e \end{bmatrix}, \quad F = \begin{bmatrix} \rho u \\ p + \rho u^2 \\ \rho u v \\ (e + p)u \end{bmatrix}, \quad G = \begin{bmatrix} \rho v \\ \rho u v \\ p + \rho v^2 \\ (e + p)v \end{bmatrix} \quad (1)$$

Here $\rho$ is the density, u and v are the velocity
components in the X and Y coordinate directions, p is
the pressure and $\gamma$ is the ratio of specific heats.
The energy per unit of volume, e, is defined as

$$e = \rho(\epsilon + \frac{u^2 + v^2}{2}),$$

where $\epsilon = \frac{p}{(\gamma-1)\rho}$ is the internal energy per unit mass.
We look for the solution of the system of equations
represented by Eq (1) in the computational domain as
shown in Fig 1 in time t, with the following
conditions at the domain boundaries:

a)  Solid wall along segment 1-2, 1-3 and 2-4
    The condition on the surface is defined by solving
    the Riemann problem between the point nearest to
    the wall in the domain of integration and its
    mirror image in the direction normal to the wall.

b)  Periodicity between segments 3-5 and 4-6
    By virtue of the central location of the channel
    flow at each grid point along 3-5 is the same as
    at corresponding grid points along 4-6 in Fig 1.

c)  Outflow along segment 5-6
    If the outflow is subsonic at the downstream
    boundary we define only the pressure $p_{out}$, and
    for all other flow parameters apply the
    continuation condition. That means that $u_{out}$,
    $v_{out}$ and $\rho_{out}$ are set equal to the values of u, v
    and $\rho$ one point ahead of the downstream
    boundary.
    If the outflow is supersonic the continuation
    condition is applied to all parameters at the
    downstream boundary.
    It is assumed that initially at the time t=0, the
channel is filled with detonation products from
segment 1-2 to 1'-2'. Outside this region of the
computational domain, the gas is assumed to be at
ambient conditions.
    The Godunov method has been used to obtain a
numerical solution of the Eq (1) with the
described boundary and initial conditions. Details of
the implementation of the method and boundary
conditions are given in (7).
    An orthogonal grid is constructed which covers
the computational domain as shown on Fig 1. It should
be noted that although the formulation of the problem
and its solution is two-dimensional, with the boundary
conditions described above the flow will be
essentially one dimensional.
    It is assumed that at t=0, the detonation wave
has passed through the combustible mixture and the
products of combustion have uniform properties. Thus
the time of initiation and propagation of the
detonation wave through the combustible mixture is
neglected in comparison with the time for propagation
through the channel and subsequent expansion of the
gases.

## RESULTS AND DISCUSSION

The history of the flow development in the diverging channel is shown in Fig 2. Here the velocity and pressure distributions at the center-line of the channel are shown at specific moments of time, where time t=0 is when the expansion begins. At time t=0, approximately 8.5% of the channel volume from the left-hand side, is filled with detonation products with initial pressure density and velocity having values of

$p_0 = 40$ atm, $\rho_0 = 5.2 kg/m^3$, $v_0 = 0$ and $u_0 = 0$ respectively. At t=0, the rest of the channel is filled with ambient air with

$p = 1$ atm, $\rho = 1.3$ $kg/m^3$, $v = 0$ and $u = 0$ . The length of the channel is 1 meter. These conditions will be referred to as Case 1.

Initially, a shock wave going from left to right and a rarefraction wave going from right to left can be seen in Fig 2. The shock wave progressively decays because the channel is diverging. The rarefraction wave propagates rapidly towards the wall at the left end of the channel, because the temperatures in this region are very high (approximately 2800 K) and the channel is converging towards the left end. At a time of about 0.15 msec the rarefraction reaches the wall at the left end of the channel. From this moment, pressure at the left end of the channel rapidly decreases from about 40 atm at $t = 0.15$ msec to about 0.3 atm at $t = 0.82$ msec. Because of this rapid depressurization of the region adjacent to the left end wall, the pressure on the right hand end of the channel becomes higher than that at the left, which generates a shock wave going from right to left at

time t=0.6 msec. This back-going shock wave rapidly slows down and then reverses the direction of the flow because the channel is converging towards its left end wall.

The negative flow reflects from the left end wall at time t=1.4 msec, forming a hammer shock wave which moves from left to right and again reverses the flow direction. The formation of the hammer shock wave can be seen clearly on the velocity and pressure graphs for time $t = 1.6$ msec. Because the shock travels in a diverging channel, it weakens rapidly.

The main shock wave produced by the detonation products leaves the channel at the time ~0.94 msec, and because the channel is diverging in the direction of propagation the pressure behind the shock wave drops from about 10 atm at time t=0.1 msec to about 5 atm, at $t = 0.94$ msec when it leaves the channel.

The mass velocity of the gas drops from about 1100 m/sec at the beginning of the expansion to about 500 m/sec when the gas begins to leave the detonation tube. The velocity of the gas leaving the tube then decreases to -20 m/sec and increases again to about 50 m/sec when the shock wave reflected from the left end wall reaches the exit of the channel. This concludes the significant events which occur in the diverging channel as a result of the expansion of the detonation products. At later times, rarefraction and pressure waves continue to form and travel in the channel, but they are much weaker and their influence on the thrust produced is very small.

In Fig 3 thrust as function of time is plotted for the case described in the graphs given in Fig 2. Thrust was calculated for the case of a stationary tube with external pressure equal to the ambient pressure using

$$F = \int_L (p_L - p_{ex}) dA_x \qquad (2)$$

It can be seen in Fig 3 that most of the thrust is produced in the 2 msec following the beginning of the expansion of the detonation products. Integration of thrust in time shows that 90% of the impulse is produced in the first 2 msec and 10% in the following 7 msec.

The peculiarities of the thrust curve can be understood in relation to the wave pattern in the tube. The first change in slope at time $t \approx 0.8$ msec corresponds to the time when the front of the main shock wave reaches the end of the tube. Because the pressure behind the shock front drops rapidly, the thrust decay increases when the main shock front leaves the channel. At time $t \approx 1.5$ msec the thrust increases as a result of the hammer shock wave reflecting from the left wall.

When the main process of expansion ends, at time $t \approx 6$ msec, the pressure in the tube is about 1.1 atm and the average density is about $0.43$ kg/m$^3$. This corresponds to an average temperature in the channel of about 935 K. Since the pressure in the tube is close to ambient, the heat exchange will be by natural convection, and it will take a relatively long time for the gas remaining in the tube after the expansion to cool.

In order to examine what will be the wave pattern and thrust when a second detonation wave expands in the channel immediately following the expansion of the first detonation wave (6 msec after the beginning of the process of expansion of the first detonation wave), conditions were simulated numerically in the following way. Results of the calculation for the first detonation wave expansion were used as the initial distributions of flow parameters. Then, in

the 8.5% of the channel volume adjacent the left end
wall the pressure, density and velocity were given the
values

$p_o = 40$ atm, $\rho_o = 5.2$ $kg/m^3$ and $v_o = u_o = 0$
respectively at time $t=0$. These conditions will be
referred to as Case 2.

In Fig 4, the thrust vs time is shown for the
second detonation wave expansion. Since the
detonation products expand in a low density hot gas,
the expansion goes much faster than in the previous
case. At time $t=0.8$ msec from the beginning of the
second detonation wave expansion, the thrust drops to
zero. This can be compared with a thrust of
approximately $6 \cdot 10^4 N/m$ at the corresponding time shown
in Fig 3, for expansion into ambient air. Then,
because the large volume of the channel has static
pressure lower than ambient, thrust becomes negative
and, as in the previous case, a back-going shock wave
develops. In Fig 5, the development in time of this
recursive shock can be followed. It is observed that
the negative flow velocities which develop are twice
as large as those for the preceding expansion into
ambient air. And at time $t=2$ msec the flow throughout
the tube is reversed. Reflection of the
left-traveling shock wave from the left end wall at
time $t=2$ msec the flow throughout the tube is
reversed. Reflection of the left-traveling shock
wave from the left end wall at time $t=2$ msec produces
a very strong hammer shock which reverses the thrust
and the flow direction at time $t=2.1$ msec. Because of
the large negative thrust, the total impulse which is
produced in Case 2 is about 15% smaller than the
impulse of the detonation products expanding in
ambient air.

Another notable effect of expansion into the
products of the previous cycle, is the substantial
rise of temperature which occurs in the channel after
the second expansion. When the process of the second
expansion ends the average temperature in the channel
is approximately 1550 K. This is 615 K higher than
the final temperature after expansion into ambient
air.

In order to examine how thrust and total impulse
are influenced by the volume of air contained at
ambient conditions in the channel before the
expansion, two additional test cases were modeled. In
Case 3, the volume of ambient air in the channel to
the right side of the interface with the detonation
products is taken to be approximately 2.5 times larger
than the volume of the detonation products. This
requires a channel about 50% shorter than the original
channel, for which the ratio of the volumes of ambient
air to detonation products was about 11. In Case 4,

there was no air in the channel when expansion began,
which implies that the channel in this case has
only about 25% of the original length. Therefore,
between Cases 3 and 4 and Case 1 only the length of
the channel was changed. The geometry of the channel,
initial parameters of the detonation products were the
same in Cases 1, 3 and 4.

In Fig 6 the thrust is shown as a function of
time for Cases 1, 3 and 4. It can be seen that Case 1
(solid line) where the channel is fully extended,
gives consistently higher thrust and that the thrust
decreases when the volume of ambient air in the
channel (or channel length) decreases. Case 3 (chain-
dotted line) and Case 4 (dashed line) have regions
where thrust is negative. Comparison of the total
impulse generated shows that the extension of the
channel is very beneficial for producing impulse. The

impulse produced in Case 4, where the tube is filled
with detonation products is $0.162 \cdot 10^3$ N/M·sec. When
the channel is extended so that only 28.6% of the
channel volume is initially filled with detonation
products (Case 3), the impulse increases 28%. An
additional extension of the channel so that only about
8.5% of the tube volume is initially filled with
detonation products (Case 1), leads to total impulse
of $0.2784 \cdot 10^3$ N/M·sec, which is a 72% increase
over Case 4.

CONCLUSIONS

Numerical modeling of the process of expansion of
detonation products in a diverging channel revealed a
flow pattern rapidly changing in time with multiple
shock and rarefraction waves. One of the most
interesting features was the occurrence of a
backwards-traveling shock wave, which developed as a
result of over-expansion in the channel. The shock
wave first reversed the flow direction (and in some
cases developed a negative thrust) and then,
reflecting from the left end wall as a hammer shock,
reversed the flow direction again, increasing the
thrust.

Modeling of the second detonation wave expanding
into the products of the previous expansion, showed
that this arrangement leads to: a) significant
negative thrust; b) increases of the gas temperature
after expansion; c) losses of 15% of the total
impulse. This leads to the conclusion that the
channel should be filled with ambient air after each
detonation and expansion. Since the process of
expansion takes only about 0.006 sec, the
time-averaged thrust which can be generated by a

single channel will be limited by the rate at which the channel can be re-charged with air and mixture, and refired. For very low initial velocities in the channel (consistent with the initial conditions specified in the modelling), the frequency of firing is limited to about 20 detonations per second. This corresponds to 0.044 sec for recharging at gas velocities of about 23 m/sec. Investigation of the influence of the channel length on the impulse and thrust production showed that increases in the volume of ambient air in the channel ahead of the detonation products, which was obtained with an increase in channel length, led to significant increases in the thrust and impulse generated during the expansion. The total impulse generated by an expansion in the channel in which 8.5% of the total volume was filled initially by the detonation products, was found to be 72% greater than in the case of a short channel filled only with the same volume of detonation products at the same initial conditions.

The diverging channel geometry provided the simplest geometry with area change to model using the unsteady 2D Godunov-Euler code. Variations in the geometry can now be made in order to examine the unsteady thrust performance.

ACKNOWLEDGMENT

REFERENCES

1. Pearson, R. D., "Pressure Exchangers and Pressure Exchange Engines," ch. 16, Thermodynamics and Gas Dynamics of I. C. Engines, compiled by D. E. Winterbone and S. C. Low, forthcoming publication.

2. Shultz-Grunow, F., "Gas-Dynamic Investigations of the Pulse-Jet Tube," NACA TM-1131, February 1947.

3. Zipkin, M. A. and Lewis, G. W., "Analytical and Experimental Performance of an Explosion-cycle Combustion Chamber for a Jet Propulsion Engine," NACA TN-1702, September 1948.

4. Nicholls, T. A.; Wilkinson, H. R. and Morrison, R. B., "Intermittent Detonation as a Thrust-Producing Mechanism," Jet Propulsion, pp. 534-541, May 1957.

5.  Dunlap, R.; Brehm, R. L. and Nicholls, T. A., "A
    Preliminary Study of the Application of
    Steady-State Detonative Combustion to a Reaction
    Engine," Jet Propulsion , pp. 451-456, July 1958.

6.  Nicholls, T. A.; Cullen, R. E. and Ragland, K. W.,
    "Feasibility Studies of a Rotating Detonation Wave
    Rocket Motor," Journal of Spacecraft and Rockets,
    vol. 3, pp. 893-898, 1966.

7.  Eidelman, S.; Colella, P. and Shreeve, R. P.,
    "Application of the Godunov Method and Higher
    Order Extension of the Godunov Method to Cascade
    Flow Modeling," AIAA-83-1941-CP, AIAA 6th
    Computational Fluid Dynamics Conference, July
    13-15, Danvers, Massachusetts, 1983.

8.  Back, L. H.; Dowler, W. L. and Varsi, G.,
    "Detonation Propulsion Experiments and Theory,"
    AIAA Journal, vol. 21, no., 10, pp. 1418-1427,
    1983.

FIGURES
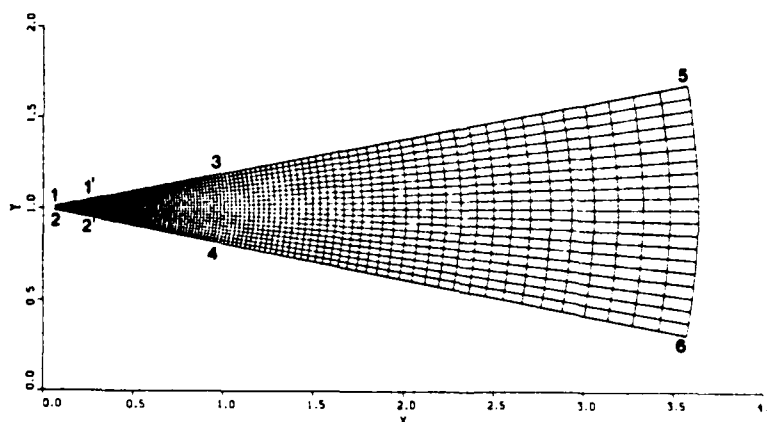


Figure 1.  The Computational Domain.
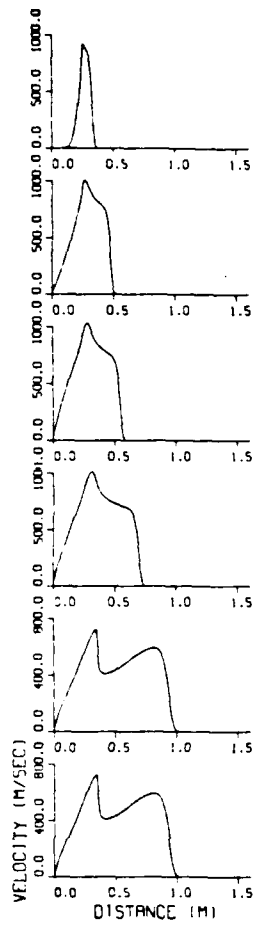
T-.07 (MSEC)

T-0.209 (MSEC)

T-.282 (MSEC)

T-.441 (MSEC)

T-.723 (MSEC)

T-.938 (MSEC)

VELOCITY (M/SEC)

DISTANCE (M)

PRESSURE (ATM)

DISTANCE (M)
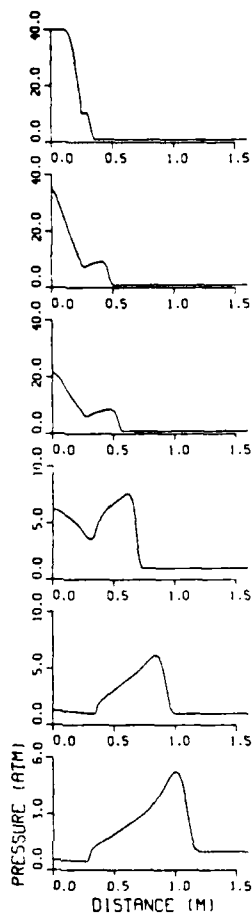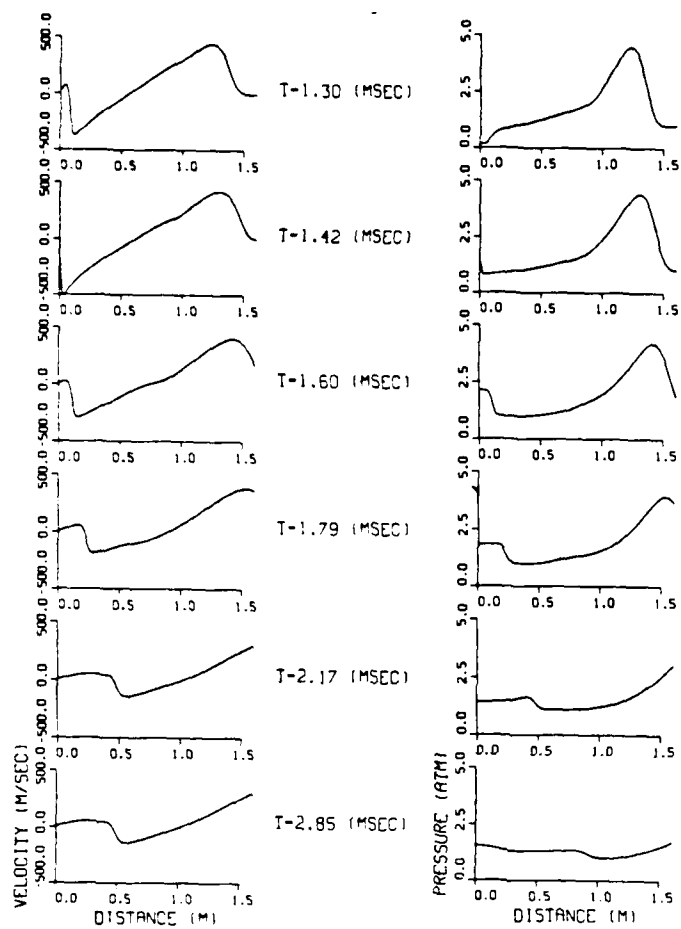
Figure 2. The Evolution in Time of the Detonation
Products Expansion.
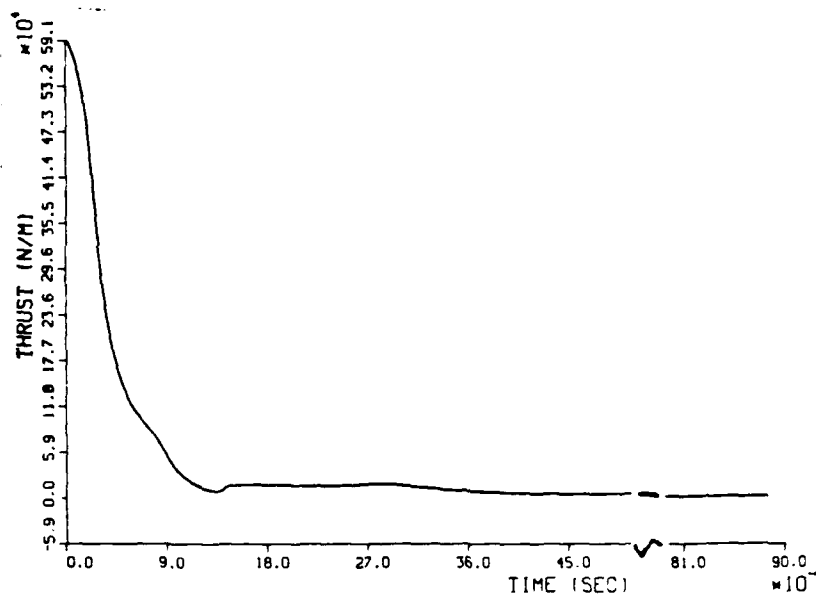
Figure 3.  The Evolution in Time of the Thrust
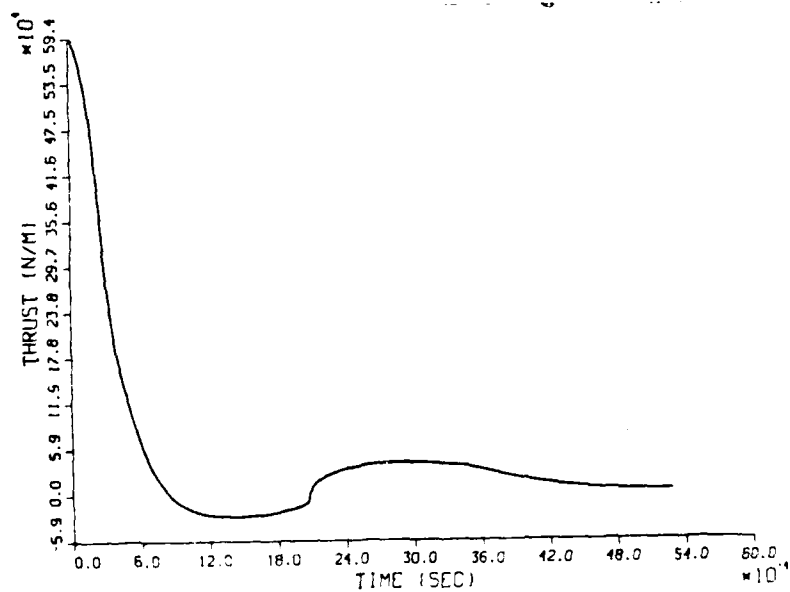Developed by the Expansion of the Detonation
Products.



Figure 4.  The Thrust vs. Time Curve for the Second
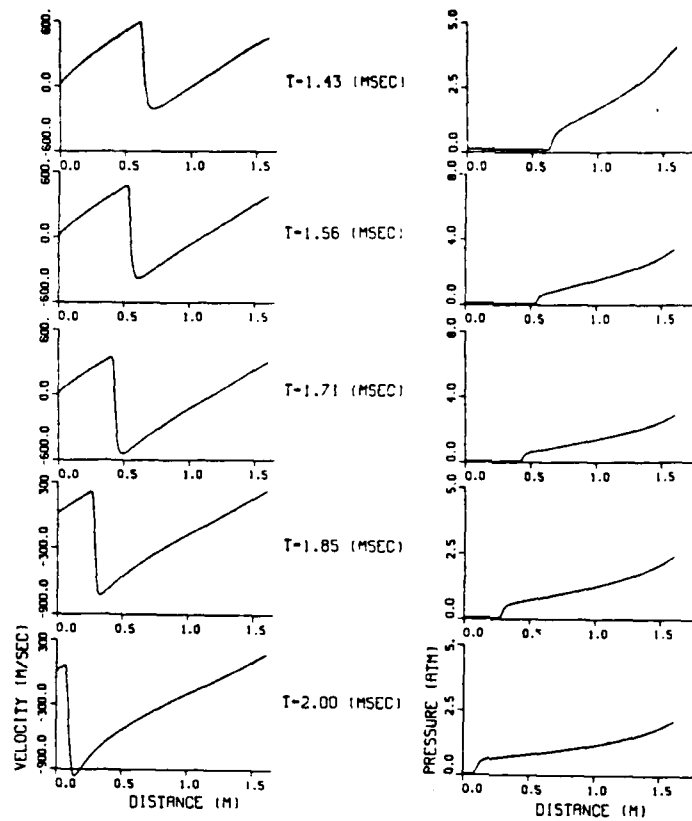Sequential Expansion of the Detonation
Products.

Figure 5.    Formation and Evolution of the Negative
             Flow Velocities for the Second Sequential
             Expansion of the Detonation Products.
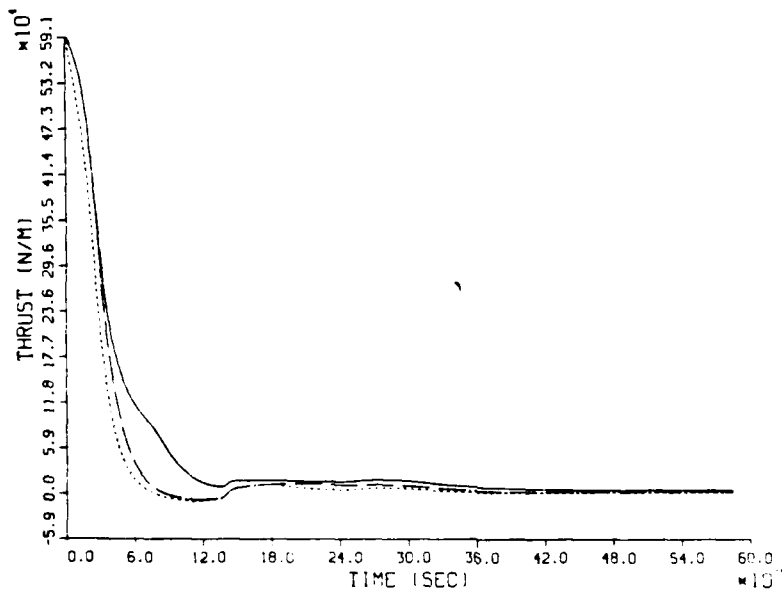


Figure 6.    The Thrust vs. Time Curves for Expansion
             in Channels of Different Lengths.
             Solid Line - Longest Channel
             Dashed Line - Shortest Channel

APPENDIX C

Numerical Techniques for Wave Rotor Cycle Analyses.

# NUMERICAL TECHNIQUES FOR WAVE ROTOR CYCLE ANALYSES

A. Mathur and S. Eidelman

Exotech, Inc.
Campbell, California  95008

R. P. Shreeve

Turbopropulsion Laboratory
Naval Postgraduate School
Monterey, California  93943

## INTRODUCTION

Wave Rotors are devices which use unsteady
pressure waves to effect direct energy exchange between
two gases. They offer the potential for significant
improvements in air-breathing engine propulsion cycles
through their capability of withstanding higher
temperatures and pressures than present-day turbines.
Other diverse applications are recounted in Ref (1).

In its most basic form, a wave rotor is a drum
with axial or helical (staggered) passages arranged
around the periphery. This single drum-like rotor
replaces separate compressor and turbine components for
gas turbine applications. The compression and
expansion of the two fluids occurs in the passages as a
result of shock tube like processes. In a typical
configuration, combustion products at high temperature
and pressure give up energy to the 'driven' fluid
(usually air) through the action of time-unsteady
compression/shock waves. The combustion products, (hot
'driver' gases), are in turn expanded and exhausted
from the rotor, the available work of expansion being
utilized to induce a fresh charge of air onto the
rotor. Careful sequencing of the passage ends past
stationary inlet and outlet ports in valve plates on
either side of the rotor creates a cyclic internal wave
pattern in the wave rotor component. The high
temperature capability of the device is a direct
consequence of the repetitive processing of both cold
and hot fluid alternately in the same rotor.

Estimation of the aero-thermodynamic performance of
these devices hinges on calculations of the unsteady
energy exchange in the wave rotor component. Numerical
simulation of the unsteady wave processes can generally
be carried out on a one-dimensional basis. However,
the complex pattern of flow discontinuities and wave
interactions known to exist in wave rotors call for
numerical methods which solve the nonlinear, hyperbolic
system of governing equations without relying on either
artificial viscosity or special treatment of
discontinuities. Described in this paper are two such
techniques, the Godunov method and a Random Choice
method (Glimm's method or Piecewise Sampling method).

## NUMERICAL FORMULATION

An essential component of both the Random Choice
method and the Godunov method is the solution of a
sequence of local Riemann problems. A Riemann problem
is defined by setting up an initial value problem for
the equations of motion in Eulerian form. The
unsteady, two-dimensional Euler equations can be
written in vectorized, conservation law form as:

$$U_t + [F(U)]_x + [G(U)]_y = 0, \text{ where } U = [\rho \ \rho u \ \rho v \ e]^T,$$

$$F(U) = [\rho u \ (p + \rho u^2) \ \rho u v \ (e + p)u]^T, \text{ and}$$

$$G(U) = [\rho v \ \rho u v \ (p + \rho v^2) \ (e + p)v]^T .$$

Here, $\rho$ is the density, u and v are the velocity com-
ponents in the x and y coordinate directions, and p is
the pressure. Subscripts indicate partial differenti-
ation with respect to that independent variable. The
energy per unit volume, e, is defined by:

$$e = \rho(\epsilon + (u^2 + v^2)/2), \text{ where } \epsilon = p/(\gamma -1)\rho$$

is the internal energy per unit mass.

The Riemann problem is intrinsically
one-dimensional in nature and is defined accordingly.
For the one space variable case, thus, $U = U(X,t)$, and
the initial value problem is set up by specifying
initial conditions which consist of intervals over
which data are constant, separated by jump
discontinuities. If the time step is chosen to be
sufficiently small, the waves propagating with finite
speeds from adjacent discontinuities remain within
their respective spatial cells and do not intersect.
This sequence of solutions from adjacent Riemann
problems is then pieced together to obtain the whole
solution at each succeeding time step.

The Random Choice method (RCM) for gasdynamics is
the outcome of a constructive existence proof of
solutions to systems of nonlinear hyperbolic
conservation laws presented by Glimm Ref (2), and its
development into an effective numerical tool by Chorin
Refs (3,4). The solution is advanced in time by a
method that includes a solution of Riemann problems as

described above and a sampling procedure, which chooses values from a representative point of the exact solution to the local Riemann problem. The sampling procedure is due to van der Corput Ref (5) and generates equidistributed sequences Ref (6). The technique eliminates numerical diffusion and flow discontinuities are computed with infinite resolution, i.e., there is no smearing.

The Godunov method is a finite difference method which computes the Riemann problem solutions as a first step, and using the fluxes thus obtained, advances in time by solving the first-order finite difference approximation of the Euler equations.

Coding details for the RCM, and the Godunov method are given in Refs (4,7) and Refs (7,8) respectively. In the following section, examples of the applications of these techniques to wave rotor devices are given.

EXAMPLE APPLICATIONS

Fig 1 shows a wave diagram (a one-dimensional space-time plot) for a wave rotor device configured to operate as a turbine alone. Air at a pressure higher than ambient enters the rotor through the inlet port, generating a shock wave with a slower moving contact discontinuity behind it at point 'a'. The shock reflects off a wall boundary at point 'b', crosses the incoming interface at point 'c' (bringing it to a halt), and reaches the inlet side again at point 'd', whereupon the inlet port is closed. The gases in the rotor passages are now in an essentially quiescent, high pressure state. At point 'e', the outlet port is opened to a lower pressure, a rarefaction fan being generated in the process. The expansion waves travel to the left, reflect off the solid boundary and propagate back to the outlet side. The port is closed when conditions in the passages are essentially the same as at the beginning of the cycle.
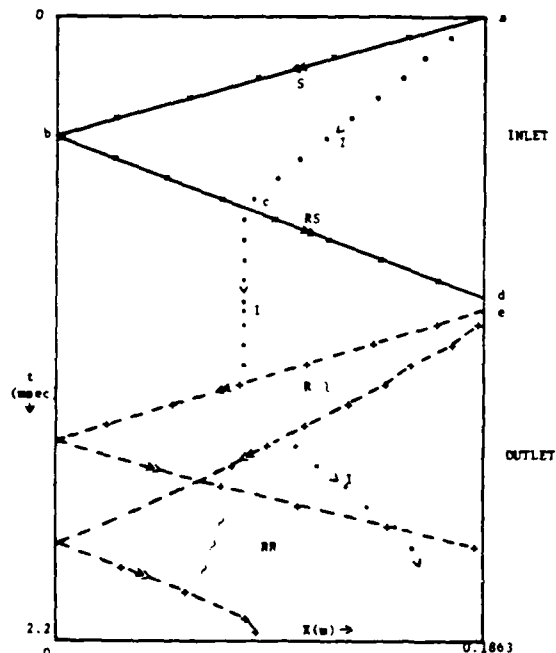


Fig. 1   Wave Diagram Computed by 1-D Random Choice Method.
S-Shock; RS-Reflected Shock; R-Rarefaction Fan; RR-Reflected Rarefaction; I-Interface

The entire wave diagram was generated by the one-dimensional sampling method with properly implemented boundary conditions. Fig 2 shows a sequence of the propagation of the shock wave and contact discontinuity in time. The perfect resolution of the discontinuities is noteworthy, even when a very small density change occurs across the interface, as in this case.
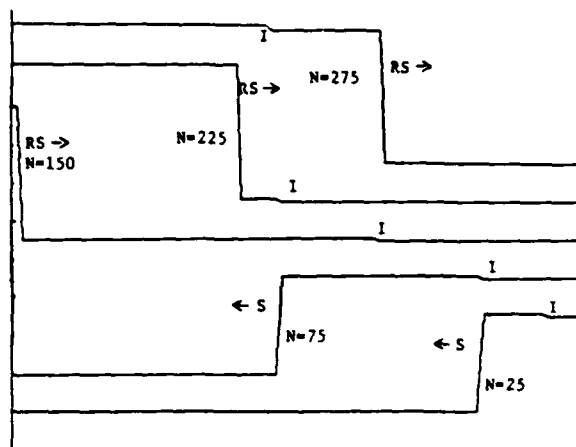


Fig. 2   Sequence Showing Shock and Interface Movement.
S - Shock; I - Interface; RS - Reflected Shock; N - Timestep

The transient process of the rotor passage end opening or closing creates losses which affect the performance of the device. The gradual (as opposed to instantaneous) opening/closing of the passages is essentially a two-dimensional flow phenomenon and is modelled using the 2-D Godunov code. Fig 3 shows a sequence of pressure contours for the gradual opening case which clearly shows the significant effect the dynamics of the passage opening has on the flow pattern in wave rotor devices. The actual shock formation for the modelled case is seen to occur approximately halfway into the passage as opposed to the instantaneous formation generally assumed for the ideal case.

DISCUSSION

The two techniques described here are powerful tools for the design of wave rotor devices. The example application of the one-dimensional Random Choice method deals with a fairly elementary wave diagram, but serves to illustrate its potential and suitability for designing complex gas turbine engine cycle type wave diagrams. The Godunov method is more amenable to extension to multidimensional analysis required for loss calculations, while fulfilling the requirements outlined in the introduction.

2

T=0.038 MSEC
T=0.073 MSEC
T=0.109 MSEC
T=0.143 MSEC
T=0.211 (MSEC)
T=0.245 (MSEC)

Y AXIS

0.00    0.02    0.04    0.06    0.08    0.10    0.12
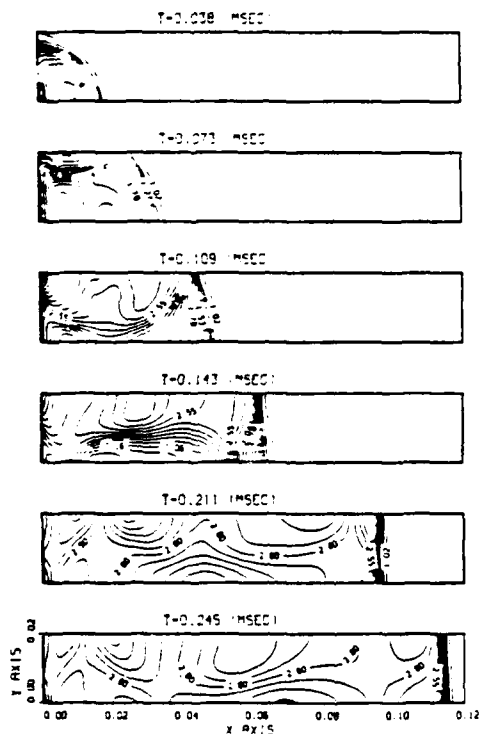X AXIS

Fig. 3  Contour Plots Generated by 2-D Godunov Method
for Gradual Opening of Wave Rotor Passage End.

REFERENCES

1.  Rose, P. H., "Potential Applications of Wave
    Machinery to Energy and Chemical Processes,"
    presented at the 12th International Symposium on
    Shock Tubes and Waves, Jerusalem, Israel, July
    16-19, 1979.

2.  Glimm, J., "Solutions in the Large for Nonlinear,
    Hyperbolic Systems of Equations," Communications
    in Pure and Applied Mathematics, No. 18, pp.
    697-715, 1965.

3.  Chorin, A. J., "Random Choice Solution of
    Hyperbolic Systems," Journal of Computational
    Physics, No. 22, pp. 517-533, 1976.

4.  Chorin, A. J., "Random Choice Methods with
    Applications to Reacting Gas Flow," Journal of
    Computational Physics, No. 25, pp. 253-272, 1977.

5.  Hammersely, J. M. and Handscomb, D. C., "Random,
    Pseudorandom and Quasirandom Numbers," Monte Carlo
    Methods, John Wiley and Sons, Inc., New York, pp.
    31-36, 1975.

6.  Colella, P., "Glimm's Method for Gasdynamics,"
    SIAM Journal for Scientific Statistical
    Computations, Vol. 3, No. 1, March 1982.

7.  Sod, G. A., "A Survey of Several Finite Difference
    Methods for Systems of Nonlinear Hyperbolic
    Conservation Laws," Journal of Computational
    Physics, No. 27, pp. 1-31, 1978.

8.  Eidelman, S., Colella, P. and Shreeve, R. P.,
    "Application of the Godunov Method and Higher
    Order Extensions of the Godunov Method to Cascade
    Flow Modelling," paper AIAA-83-1941-CP, presented
    at AIAA 6th Computational Fluid Dynamics
    Conference, Danvers, Massachusetts, July 13-15,
    1983.

APPENDIX D

Local Cell Orientation Method - Illustration of the Method for the Solution
with an Oblique Shock.

Local Cell Orientation Method.

Illustration of the method for the solution with oblique shock

## INTRODUCTION

The Finite Volume Schemes for numerical solution of the Euler equations can be split into two main steps:

   a)Calculation of the fluxes on the cell edges;

   b)Updating the values at the center of the cell ,using the
      calculated fluxes, to satisfy the Euler conservation laws.

Usually the accuracy of the flux calculation determine the accuracy of the numerical modeling Ref.1. In the region of the shock wave the accuracy of the flux calculation is significantly reduced and in some methods special care should be taken in order to reduce the pre-shock and after-shock oscillations.When the upwind methods are used the fluxes are usually calculated using the one dimensional wave propagation problem (i.e. Riemann problem). In this case the assumption of the one-dimensionality lead's to large computational errors and significant shock smearing in the region of the oblique shock.

In the current study it will be demonstrated that the accuracy of the numerical modeling could be significantly improved by proper Local

Cell Orientation (SELCO Method). We applyed the SELCO Method only with the Godunov scheme for the solution of the Euler equations, but the idea of the method is general enough to be used with other finite volume methods.

## THE SELCO METHOD.

For the Godunov method the numerical fluxes are calculated using the solution of the Riemann problem. First the solution is assumed to be piece-wise constant in every cell. Then, to calculate the flux for every cell edge the Riemann problem is solved between the cells adjacent to the edge. Solution of the Riemann problem is obtained in the direction normal to the cell's edge. The equations are then integrated in the each cell for one time step using the finite difference approximation of the Euler equations and the fluxes at the cell's edges. A more complete description of the Godunov method can be found in Ref.1.

In the two dimensional Godunov method it is assumed that the fluxes could be determined using the solution of the one dimensional Riemann problem if the CFL number used is smaller than 0.5. In the following example it will be demonstrated that that assumption lead's to consider- able errors for the solutions with oblique shock waves.

As a test case the supersonic flow over the 22.3° wedge was simu- lated. The grid and the computational domain is shown on the Figure 1. The system of the two dimensional Euler equations as in Ref.1, was solved by time marshing in the computational domain shown in Fig.1 for

time t→∞ with the following conditions at the domain boundaries:

      a) Inflow of the air at M=2.2 along segment 1-2;

      b) Outflow along segment 3-4;

      (the flow along this segment will be supersonic and

      the continuation condition is applied to all parameters

      at the downstream boundary)

      c) Solid wall along segments 1-3 and 2-4.

In the Figure 2 (a,b,c,d) results of the flow simulation using the Godunov method in the computational domain shown on Fig.1 (squares) are compared with the analytical solution for the supersonic flow over the wedge (solid lines) Ref.2. Comparison is done for the data on the *lower surface of the channel* shown on the Fig.1. It can be concluded from this comparison that only pressure coefficient is calculated accuratly by the Godunov method. Especially notable the error in entropy. Exact entropy change on the shock wave is 2 times smaller than that predicted by the Godunov method. The isomach lines are shown for the same simulated case, in Figure 2 (e). The shock is smeared over the large area of the mesh (up to 5-6 points), but the shock's angle is simulated correctly.

In order to study the source of errors for this type of problems the supersonic flow over the wedges with different angles was simulated. It was found that the pressure was predicted accuratly for the all simulated cases. At the same time the error in entropy increases when the shock wave obliquity increases. Dependence of the accuracy of the shock simulation on the shock obliquity is not surprising since the basic

assumption about independance of the flux calculation for the intersecting edges of the cell, for  t < 0.5*CFL, became incorrect in the vicinity of the shock.  Spliting the flux calculation for each cell on four one dimensional Riemann problems for each of the cell's edges would not lead to the large errors in the regions of monotonic flow. It will also give accurate approximation in the region of the oblique shock *if the shock wave is parallel to one of the cell edges*.  The last statement will be illustrated by the following numerical example.

Let's solve the problem of the supersonic flow with M =2.2 over the 22.3° wedge, as in previous example, on the grid shown in Figure 3. The grid in Fig.1 is skewed uniformly so that vertical lines of the grid are forming a 51.7° angle with the positive direction of the x-axis.  An angle of 51.7° corresponds to the shock wave angle calculated analytically Ref.2. Because the grid is skewed the oblique shock waves will be parallel to the vertical grid lines of the mesh shown in Fig.3. Results of this test case, in the form of the distribution of pressure coefficient, entropy, density and velocity, are compared to the analytically calculated values (solid lines) in Figure 4 (a,b,c,d). In  Fig.4 (e), the isomach lines for this simulation are shown. It can be concluded from the results presented in Fig.4, that the flow is modeled is this case with very high accuracy. Shock wave is resolved on one grid cell and entropy jump is calculated exactly.  All that is result of the proper cell orientation towards the shock wave.

Skewing the entire grid can help to accuratly resolve only one shock wave, and only on the condition that the shock wave angle is known prior to the solution, so it could not be applied effectivly. But

if skewing of the cell can be done locally in the region of the oblique shock it can improve the accuracy of the shock wave simulation.

The proposed SELCO method does the cell reorientation locally. The method consist from the following steps:

1) Integration of the Euler equations by the Godunov method;

2) Define the approximate shock location and the shock angle using the expressions for oblique shocks Ref.2.
(Based on the fact that pressure is calculated accuratly by the Godunov method);

3) Rotate the cell edges that are directed along the shock about their middle points on the shock wave angle. So, after rotation, two of the cell edges will be parallel locally to the shock wave surface (see Figure 5);

4) Calculate the fluxes on the new edges of the cell;

5) Integrate the Euler equations in the new cell.

All these additional steps do not add much of computational work, because the cell reorientation should be done only in the vicinity of the shock wave. If the shock could be resolved on one grid point, only one cell would be transformed. Our experience has shown that there is no need to extend the SELCO procedure on the cells ahead and behind the shock wave surface.

In Figure 5 (a,b,c,d) results are shown for the same flow condition as in previous cases: supersonic flow with $M_\infty = 2.2$ over the wedge of

22.3°. Calculations were done on the grid shown in Figure 1 and in this case the SELCO method was applyed. It can be concluded from the results presented in Fig. 5 that the accuracy of the shock wave modeling using the SELCO method approach that demonstrated in Figure 4 for the completely skewed grid, and is superior to the accuracy of the standard Godunov method. The isomach lines for the case where the SELCO method was applied are presented in Figure 5 (e). The shock tickness in this graph is minimal and much more improved compared to the simulation by the original Godunov method shown in Figure 2 (e).

## CONCLUSIONS.

It has been demonstrated that inaccurate modeling of the oblique shock waves produced by the Godunov method is the result of the obliqueness of the shock wave with respect to the edges of the cells of the computational grid covering domain of integration. It is also shown that only when the shock surface is parallel to the two opposite edges of the cell the oblique shock can be accuratly calculated.

A new method of the Local Cell Orientation (*SELCO Method*) is proposed in order to allow local reorientation of the cells in the vicinity of the shock waves. The efficiency of the SELCO method is demonstrated for the simulation of the oblique shock waves in the supersonic flow using Euler equations.

Although the new SELCO method was demonstrated with the Godunov scheme it will be effective in applications to the other upwind methods

that use the finite volume formulation.

## ACKNOWLEDGEMENT

## REFERENCES

1. Eidelman, S., Colella, P., and Shreeve, R.P., "Application of the Godunov Method and Higher Order Extention of the Godunov Method to Cascade Flow Modeling," paper AIAA-83-1941-CP, presented at AIAA 6th Computational Fluid dynamics Conference, Danvers, Massachusetts, July 13-15, 1983.

2. Equations, Tables, and Charts for Compressible Flow, Ames Aeronautical Laboratory, NACA Report 1135, 1953.

FIGURE CAPTIONS.

1. The Computational Domain.

2. Computation by the Godunov method. $M_\infty$=2.2.

   Wedge Angle is 22.3°. Continuous lines
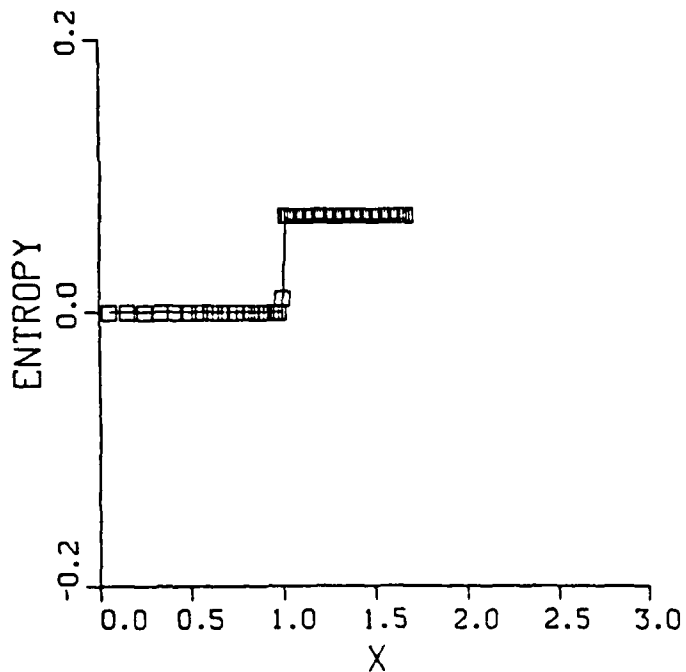
   show the exact solution for - a,b,c and d.

   a) Surface Pressure Coefficient.

   b) Surface Entropy.

   c) Surface Density.

   d) Surface Mach Number.

   e) Isomach Lines.

3. The Computational Domain with the Skewed Grid.

4. Computation by the Godunov Method on the Skewed Grid Shown

   in Figure 3. $M_\infty$=2.2. Wedge Angle is 22.3°.

   Continuous lines show the exact solution for - a,b,c and d.

   a) Surface Pressure Coefficient.

   b) Surface Entropy.

   c) Surface Density.

   d) Surface Mach Number.

   e) Isomach Lines.

5. The Local Cell Reorientation by the SELCO Method.

6. Computation by the SELCO Method. $M_\infty$=2.2.

   Wedge Angle is 22.3°. Continuous lines

   show the exact solution for - a,b,c and d.

   a) Surface Pressure Coefficient.

   b) Surface Entropy.

   c) Surface Density.

   d) Surface Mach Number.
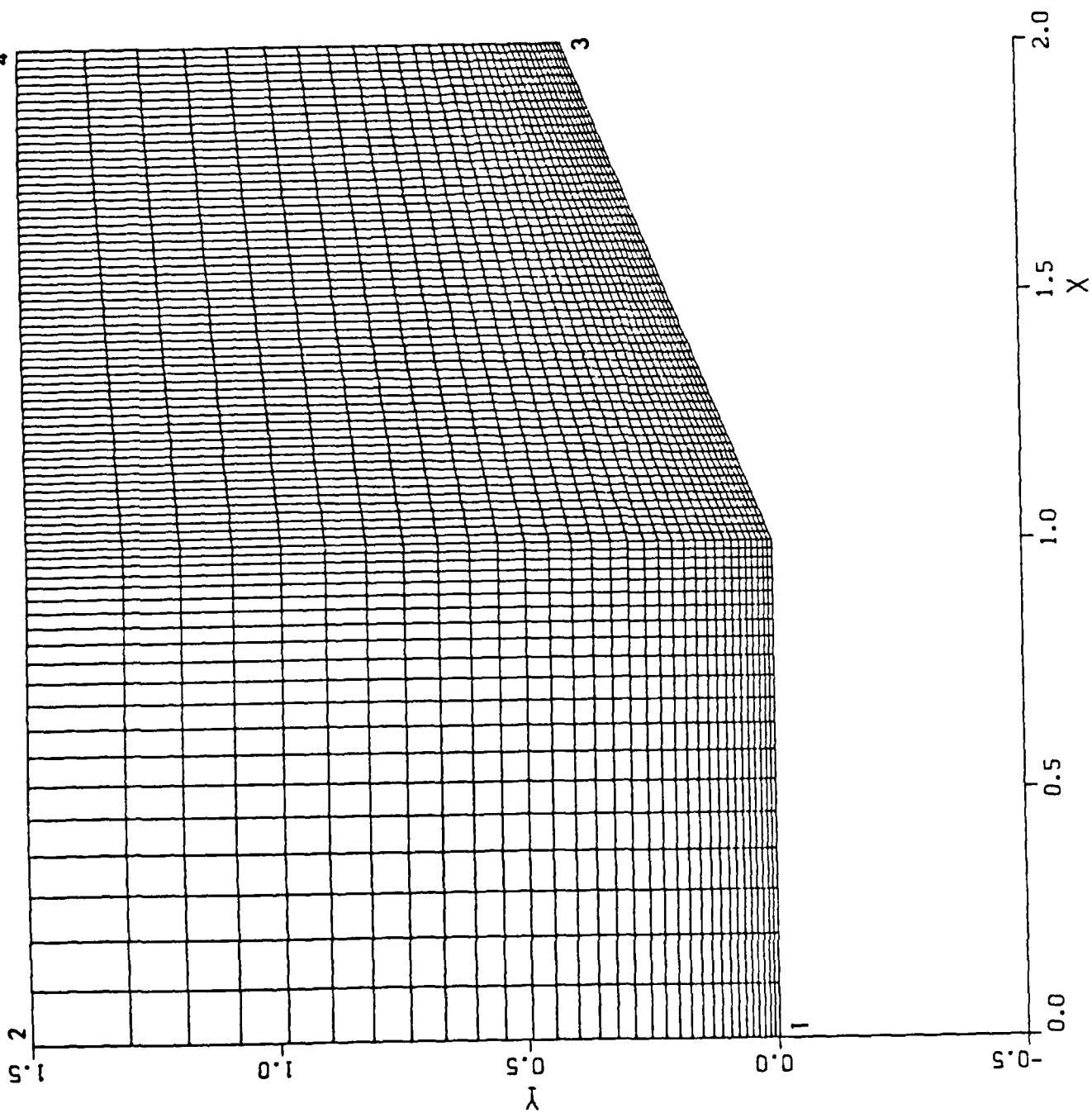
   e) Isomach Lines.

1. The Computational Domain.
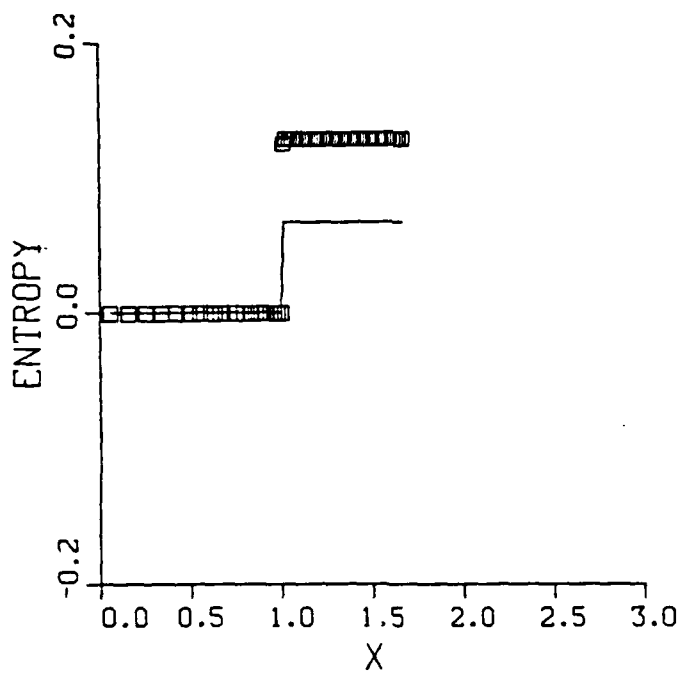
b) Surface Entropy.
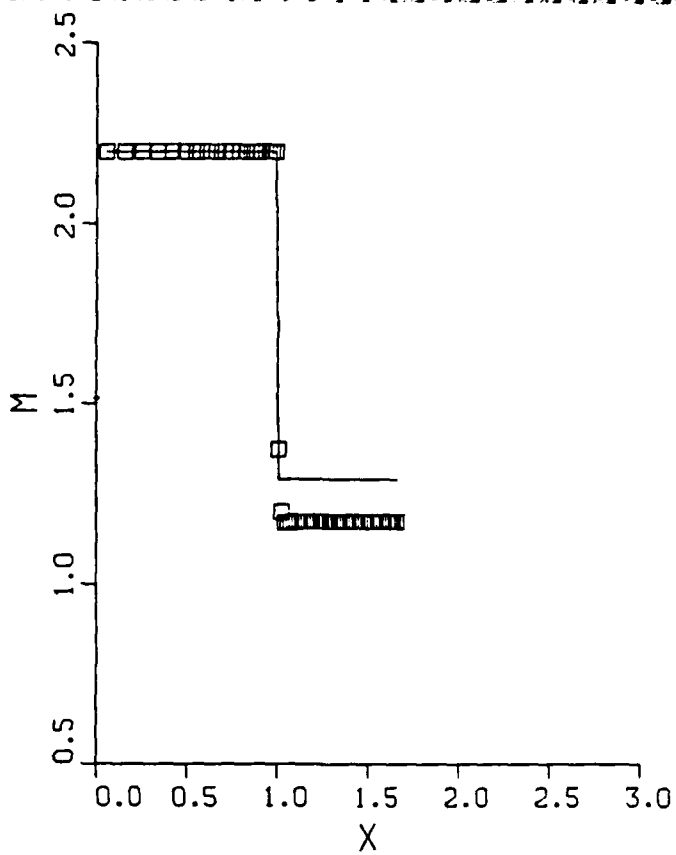
d) Surface Mach Number.
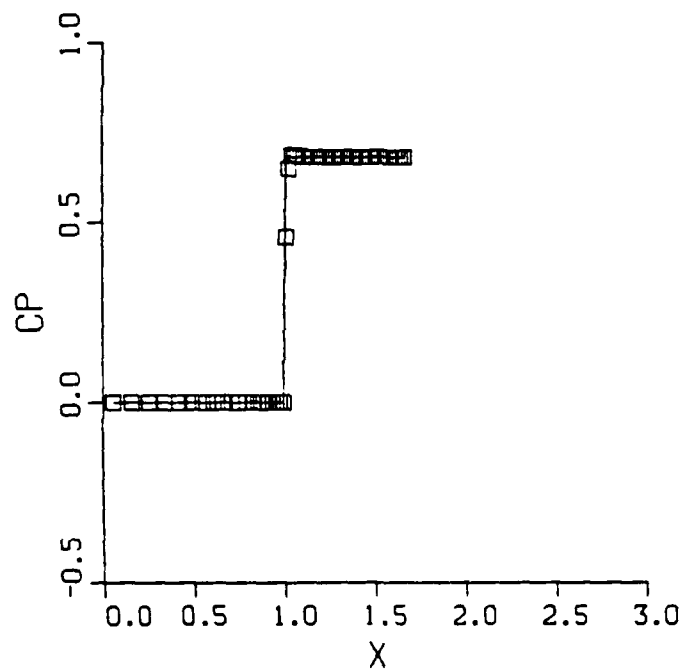
a) Surface Pressure Coefficient.
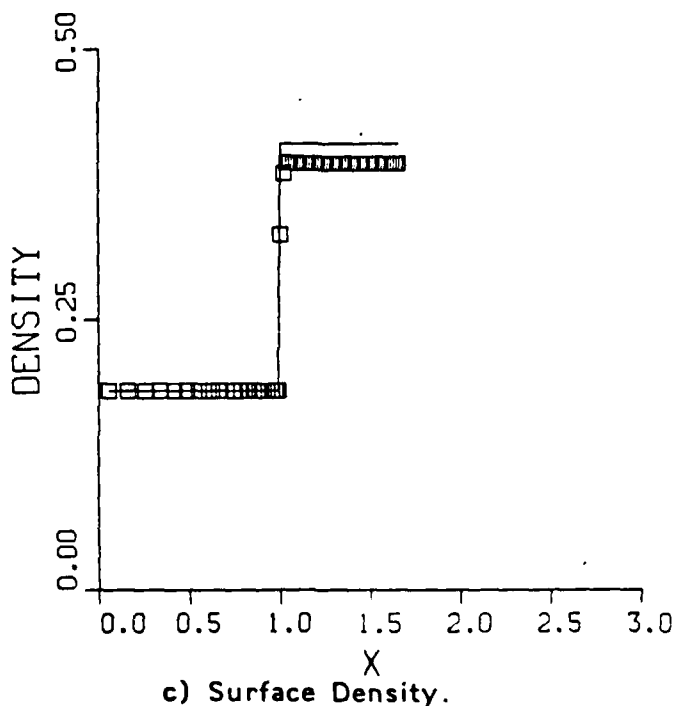
c) Surface Density.

2. Computation by the Godunov method. $M_\infty = 2.2$.

Wedge Angle is $22.3°$. Continuous lines

show the exact solution for - a,b,c and d.
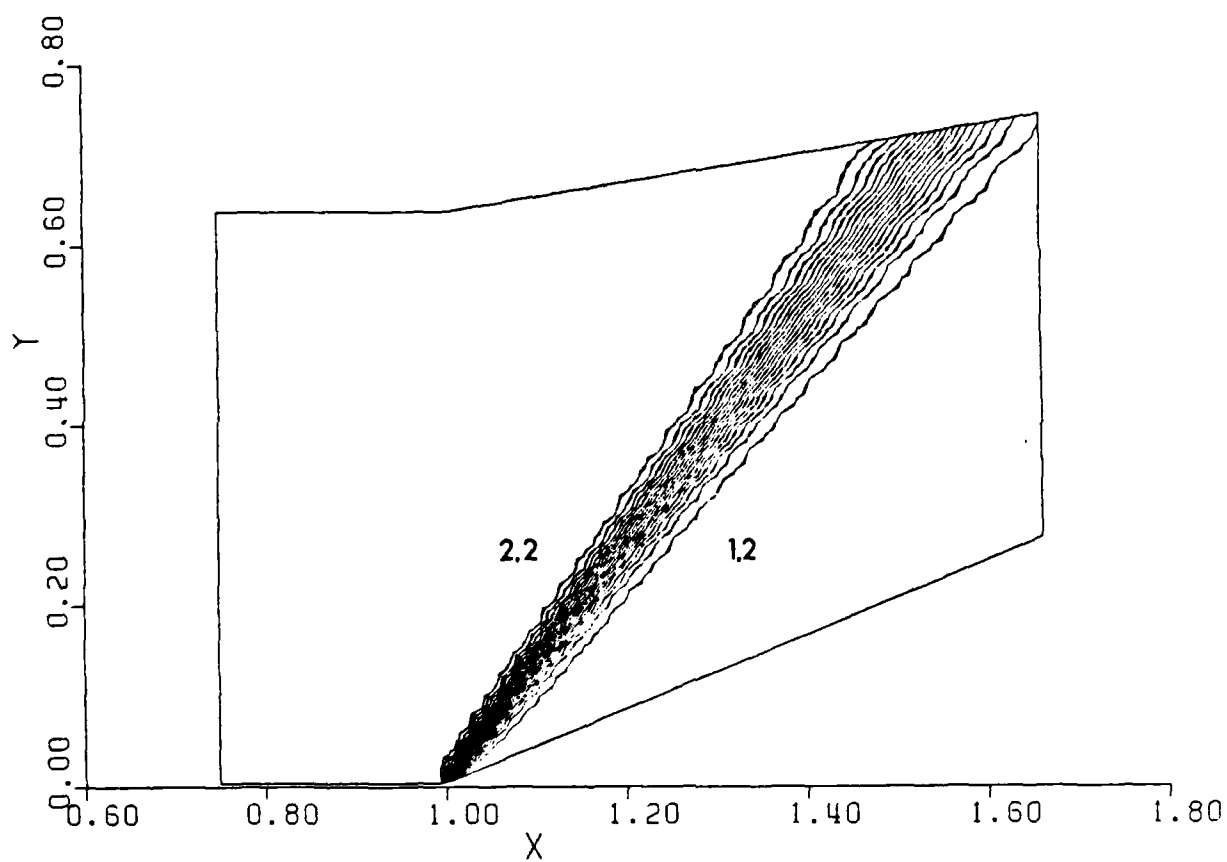
e) Isomach Lines.

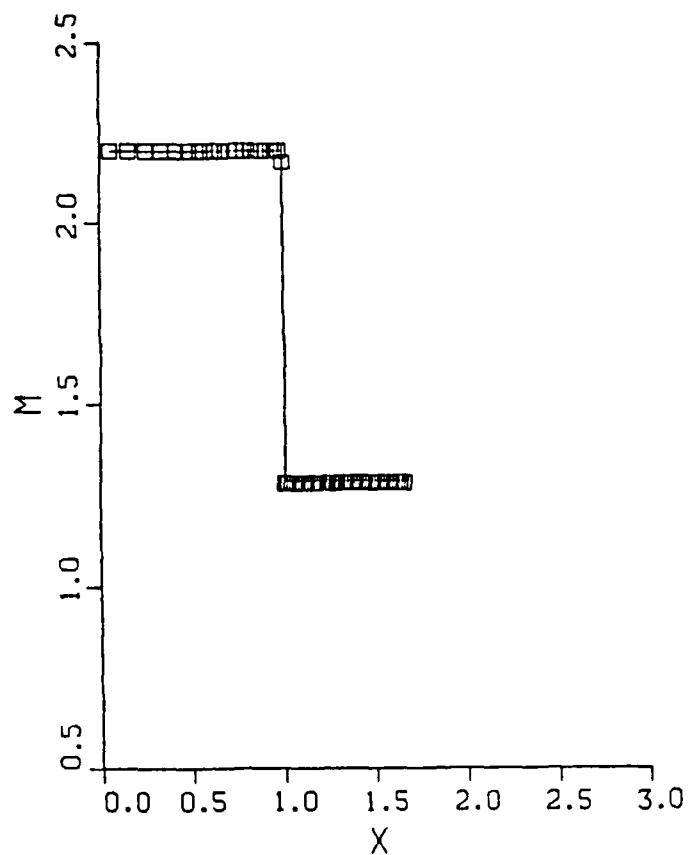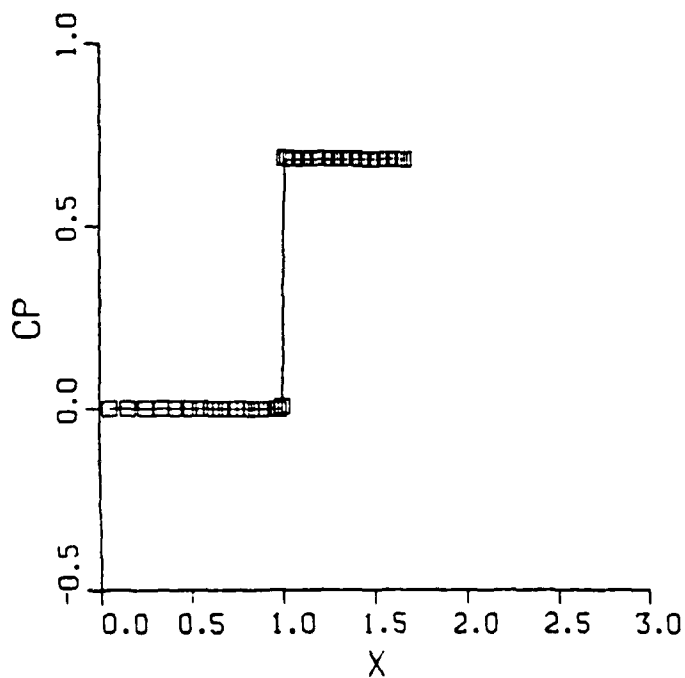2. Computation by the Godunov method. $M_{-\infty}$=2.2.
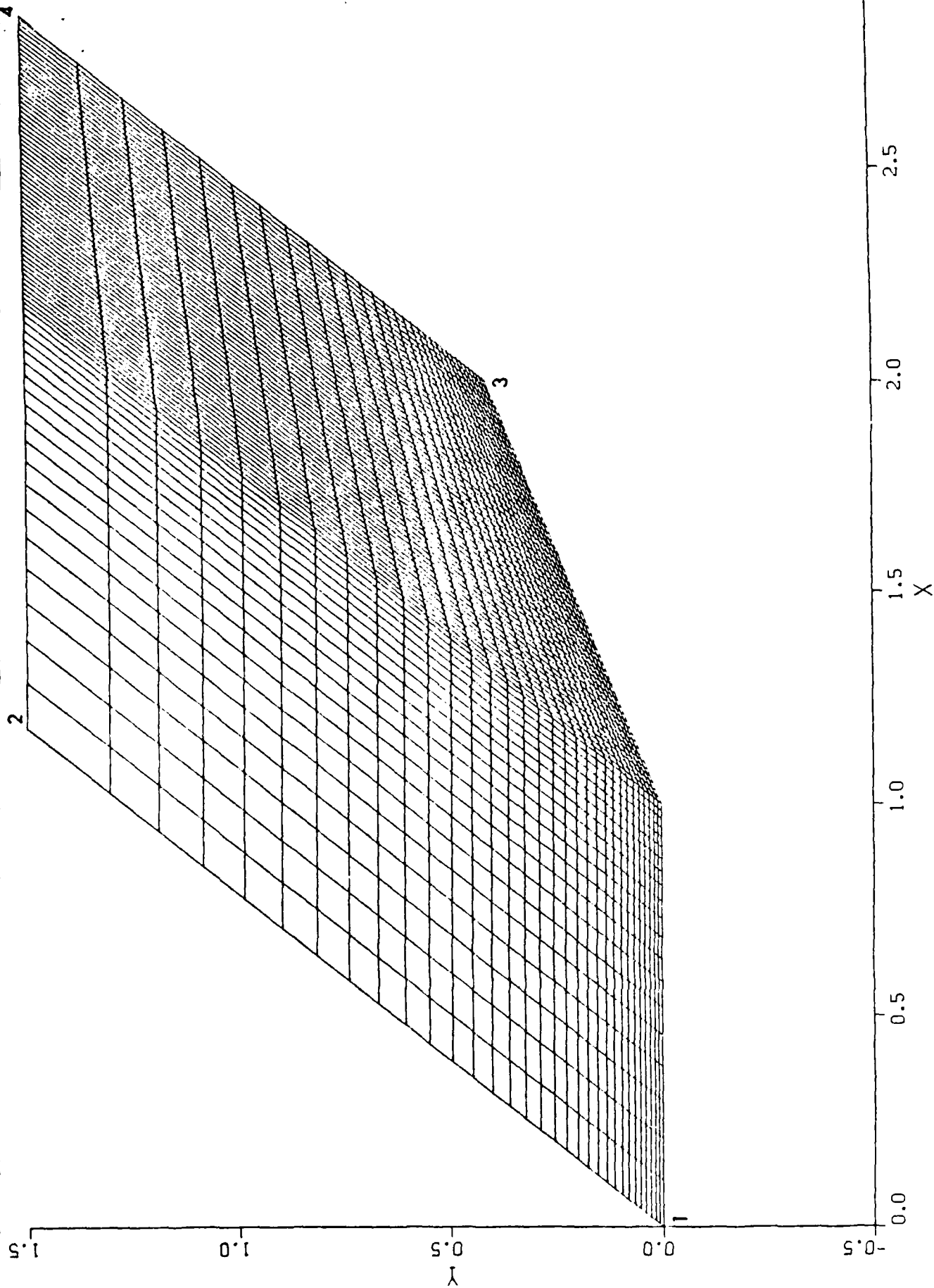
Wedge Angle is 22.3°.
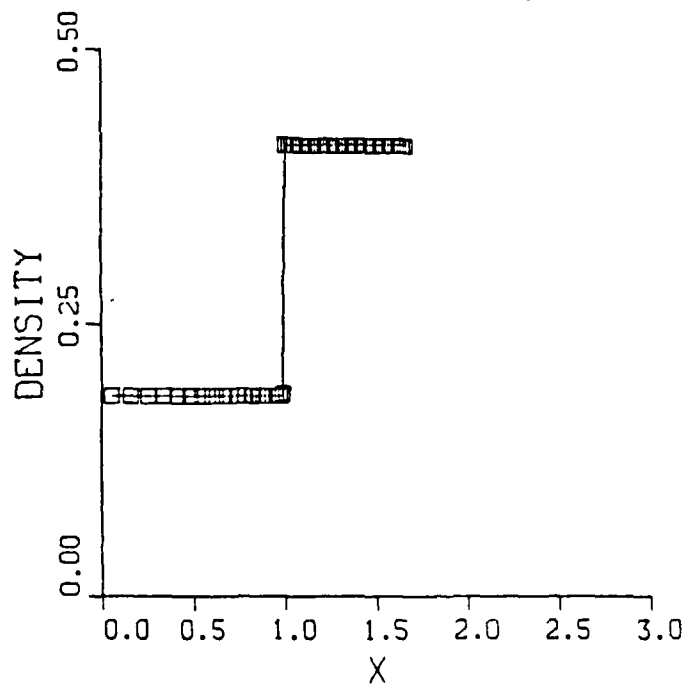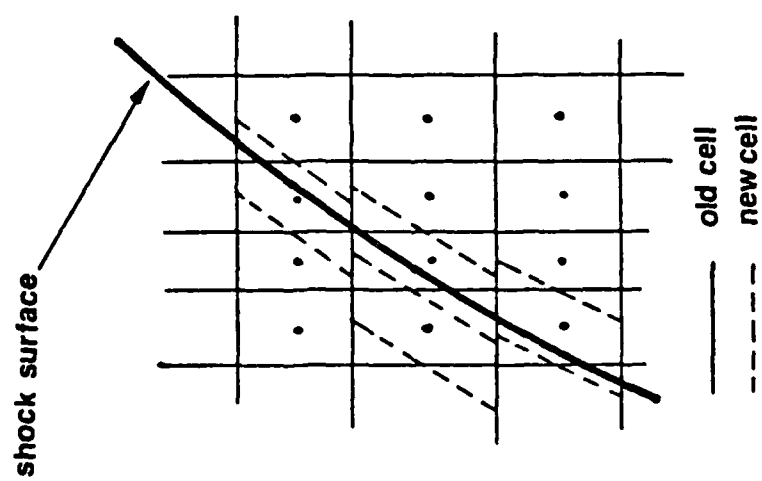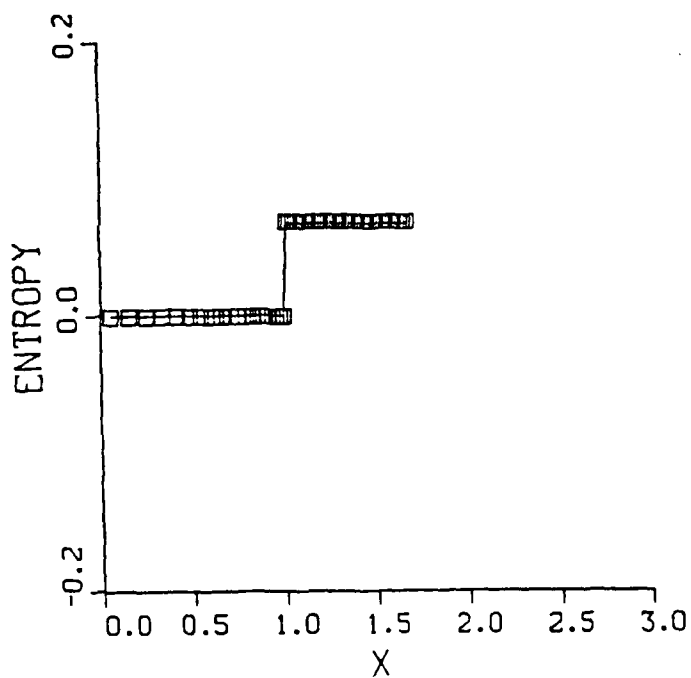
3. The Computational Domain with the Skewed Grid.

b) Surface Entropy.

d) Surface Mach Number.

a) Surface Pressure Coefficient.

c) Surface Density.

4. Computation by the Godunov Method on the Skewed Grid Shown
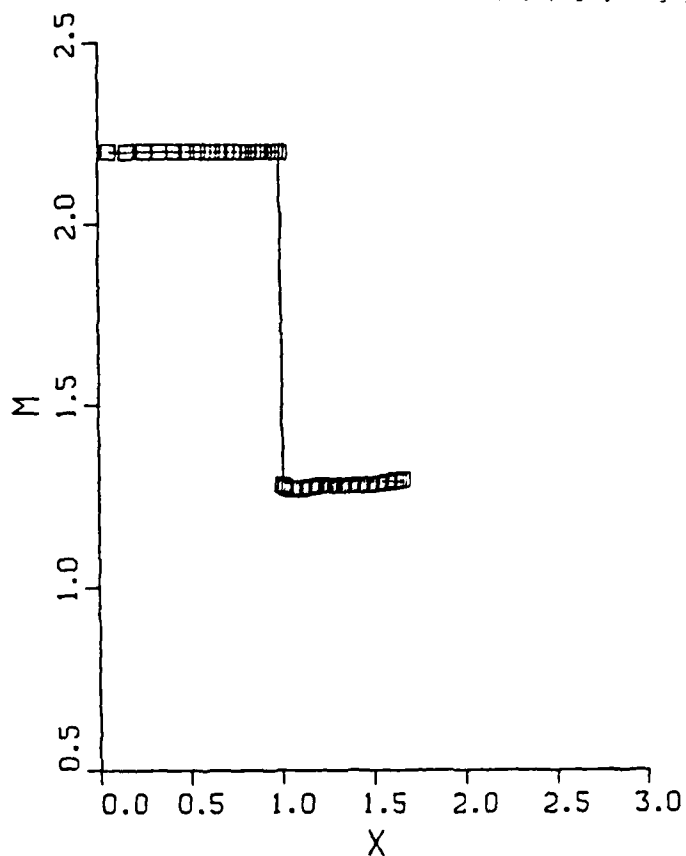
in Figure 3. $M_\infty$=2.2. Wedge Angle is 22.3°.

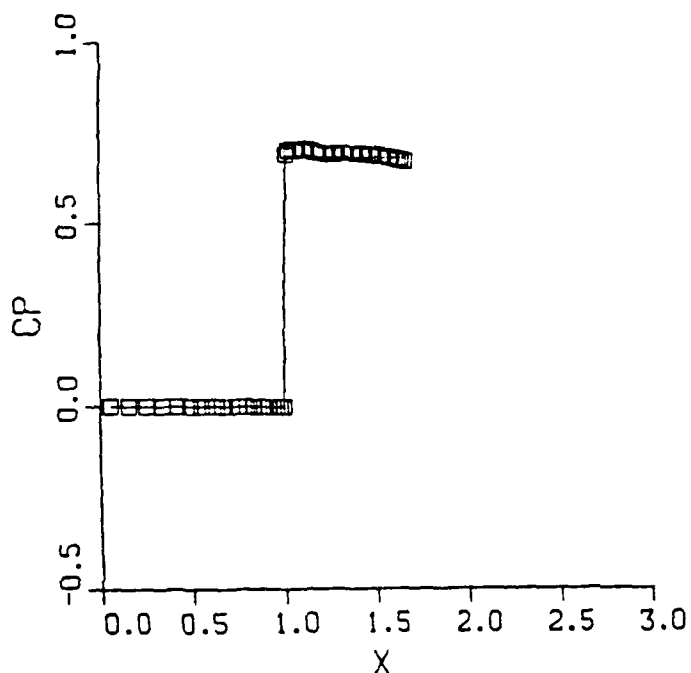Continuous lines show the exact solution for - a,b,c and d.
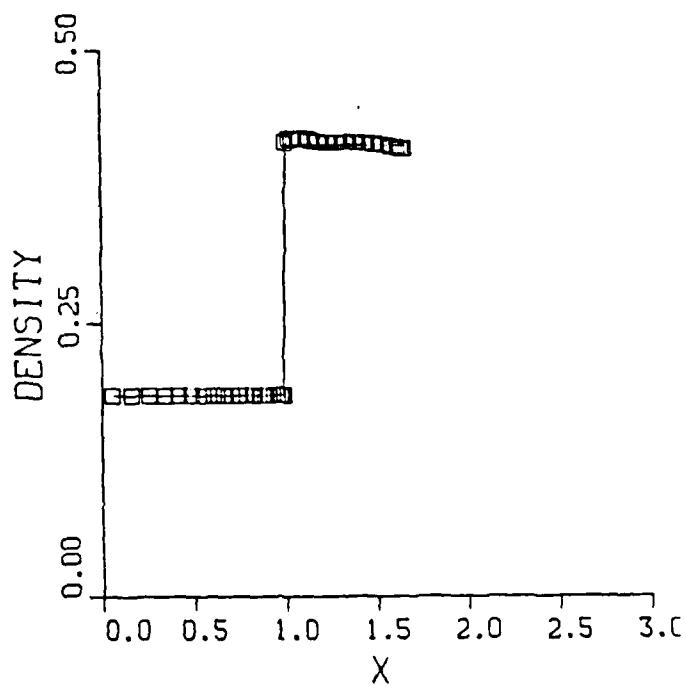
5. The Local Cell Reorientation by the SELCO Method.

b) Surface Entropy.

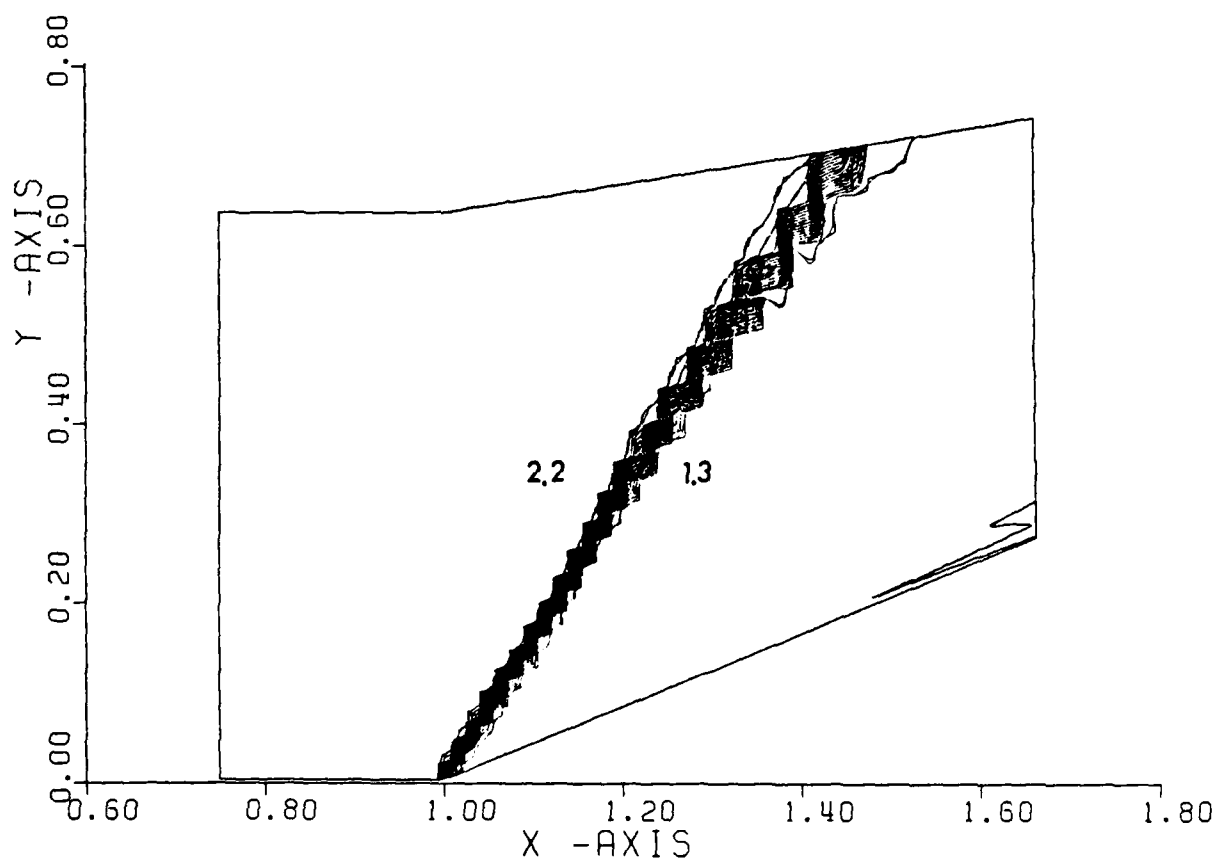d) Surface Mach Number.

a) Surface Pressure Coefficient.

c) Surface Density.

6. Computation by the SELCO Method. $M_{\infty}$=2.2.

Wedge Angle is 22.3°. Continuous lines

show the exact solution for - a,b,c and d.

e) Isomach Lines.

6. Computation by the SELCO Method. M = 2.2.

Wedge Angle is 22.3°. Continuous lines

# END
# FILMED

5-86

# DTIC